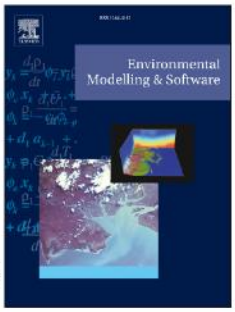

A satellite-driven hydro-economic model to support agricultural water resources management

M.P. Maneta, J.S. Kimball, M. He, N.L. Silverman, B.C. Chaffin, B. Maxwell, S. Ewing, K. Cobourn, X. Ji

PII: S1364-8152(20)30893-8

DOI: https://doi.org/10.1016/j.envsoft.2020.104836

Reference: ENSO 104836

To appear in: *Environmental Modelling and Software*

Accepted Date: 6 August 2020

Please cite this article as: Maneta, M.P., Kimball, J.S., He, M., Silverman, N.L., Chaffin, B.C., Maxwell, B., Ewing, S., Cobourn, K., Ji, X., A satellite-driven hydro-economic model to support agricultural water resources management, *Environmental Modelling and Software*, https://doi.org/10.1016/j.envsoft.2020.104836.

A SATELLITE-DRIVEN HYDRO-ECONOMIC MODEL TO SUPPORT AGRICULTURAL WATER RESOURCES MANAGEMENT

Maneta M.P.[1,*], Kimball, J.S., He, M., Silverman, N.L.

Geosciences Department, University of Montana, Missoula, MT

Chaffin, B.C.

W.A. Franke College of Forestry and Conservation, University of Montana, Missoula, MT

Maxwell, B., Ewing, S.

Land Resources and Environmental Sciences, Montana State University, Bozeman, MT

Cobourn, K.

Department of Forest Resources and Environmental Conservation, Virginia Tech, Blacksburg, VA

Ji, X.

Department of Economics and Environmental Studies Program, Brandeis University, Waltham, MA

Abstract

The management of water resources among competing uses presents a complex technical and policy challenge. Integrated hydro-economic models capable of simulating the hydrologic system in irrigated and non-irrigated regions including the response of farmers to hydrologic constraints and economic and policy incentives, provide a framework to understand biophysical and socioeconomic implications of changing water availability. We present a transformative hydro-economic model of agricultural production driven by multi-sensor satellite observations, outputs from regional climate models, and socioeconomic data. Our approach overcomes the limitations of current decision support systems for agricultural water management and provides policymakers and natural resource managers with satellite data-driven, state-wide, operational models capable of anticipating how farmers allocate water, land, and other resources when confronted with new climate patterns, policy rules, or market signals. The model can also quantify how farming decisions affect agricultural water supplies. We demonstrate the model through an application in the state of Montana.

Keywords: hydro-economic models, positive mathematical programming, data assimilation, decision support systems

Software availability

The Python modeling package presented in this work is available free of charge through the BitBucket repository `https://bitbucket.org/umthydromodeling/dawuap.git` (version 0.1beta). The data assim-

*Corresponding author

ilation Water Use and Agricultural Productivity (daWUAP) package was developed by Marco Maneta (marco.maneta@umontana.edu) and was made publicly available in April 2020. The package is written in pure Python version 3.7 and has been tested within the Anaconda Python environment on Linux and Mac OSX operating systems.

1. Introduction

Many productive agricultural regions in the world are characterized by highly variable inter-annual precipitation, groundwater supplies, and stream flows. This is already increasing, and expected to continue in an upward trend as climate changes (Groisman and Easterling, 1994; Easterling et al., 2000; McCabe and Clark, 2005; Mote, 2006; Long et al., 2013). Correspondingly, more frequent and intense droughts and more severe storm and runoff events will present new challenges for water managers (Harou et al., 2006; Gorelick and Zheng, 2015). As opportunities to develop new water supplies decline, managers will need to improve the efficiency of the existing sources to satisfy growing demands (US Army Corps of Engineers and US Army Corps of Engineers, 2012).

Agriculture has a long history of adapting to variability in local conditions (McCarl, 2015; Rose, 2015). Evidence to date suggests that farmers have met these challenges by changing their water allocations, crop mix, and land use practices (Schneider et al., 2000; Bryant et al., 2000; Menzel et al., 2006). However, little is known about how farmer adaptation alters natural hydrologic systems, impacts water users downstream, and how policy instruments encourage or impede adaptation (White et al., 2011).

Regional resource managers rely on modeling tools to inform decision making, including hydro-economic models that simulate the balance between the regional water supply system and anticipated demands from agricultural producers under a range of scenarios. Hydro-economic models are integrated tools that incorporate the realities of water management systems, including variable spatial impacts and dynamic demands influenced by economic and policy drivers (Harou et al., 2009). These types of models have been a subject of research since the late 1990s (Pulido-Velazquez et al.; Ward and Lynch, 1996; Cai et al., 2003; Ward et al., 2006; Cai et al., 2008; Brouwer and Hofkes, 2008; Medellín-Azuara et al., 2011; Elbakidze et al., 2012, 2018), and are one of the most promising tools for future integrated water management. The research applications of these models capture the spatial and temporal inter-dependency between water supply and demand in a hydro-economic system; in operational water management applications, however, they often do not incorporate these internal feedback mechanisms. Another limitation of current operational water management models is that they typically neglect the spatially-explicit and dynamic nature of human actions, often assuming that the behavior of one farmer does not affect the choices of other farmers downstream. However, upstream decision-making is likely to influence the availability of water for downstream uses and the ability of downstream farmers to adapt to climate change (Maneta et al., 2009a,b).

Adaptive behavior and spatially-dynamic processes are rarely simulated because they are difficult to

human behavior into hydro-economic models using a constrained optimization approach with farmer response functions calibrated to reflect previously observed decisions. This optimization approach is followed by models calibrated using the Positive Mathematical Programming (PMP) method (Howitt, 1995). Models calibrated using PMP have been widely applied to understand and optimize agricultural water allocation and for policy analysis (Maneta et al., 2009b; Medellín-Azuara et al., 2008; Torres et al., 2011; Ghosh et al., 2014; Kahil et al., 2015; Heckelei et al., 2012; Graveline and Merel, 2014; Connell-Buck et al., 2011; Medellín-Azuara et al., 2011; US Bureau of Reclamation, 2011; Department of Water Resources, 2009; Cobourn and Crescenti, 2011), and can represent farmer behavior at a fraction of the complexity and computational requirements of other popular alternative approaches such as statistical, econometric or agent-based models (Wurster et al., 2019; Ng et al., 2011; Weersink et al., 2002). An additional advantage of this approach is that the calibrated hydro-economic models are more amenable to coupling with physically-based models that represent the distributed regional hydrologic system. This coupling is key to tracing the effects of farmer adaptation on natural systems over space and time.

PMP is a well-established method of calibrating hydro-economic models, but its predictive capability hinges on the quality and quantity of the data that it uses to reflect observed farmer behavior. The popularity of programming methods in operational hydro-economoic models has to some extent been limited by the availability of high-quality data for calibration, which is often derived from survey data collected on producer behavior. Due to the relatively high cost of administering surveys, data collection efforts necessary to calibrate and refine hydro-economic models are often focused on specific watersheds, limiting the transferability and utility of these models. Among other problems, if a surveyed sample of farmers or the specific year of the survey are not representative of a broader set of producers and long-term conditions, the calibration may have a bias toward a spatially- and temporally-narrow set of farm conditions. An opportunity to overcome this limitation is to use satellite-based remote sensing observations of agricultural activity spanning multiple years of recorded data. The increased availability of high spatial resolution, remotely-sensed time-series data, allows for classification of crop types and land allocation trends (USDA NASS, 2015), retrieval of vegetation productivity information including for specific crops (He et al., 2018; Mu et al., 2009), and estimation of vegetation water use (He et al., 2019; Zhang et al., 2010; Allen et al., 2007) at a finer spatial and temporal scale, and across a broader geographic scope, than has been possible to date using survey instruments.

Although remotely-sensed data are subject to greater noise than survey data, remote sensing retrievals of agricultural activity provide continuous annual observations over a long period of time and over large geographic extents. Stochastic recursive data assimilation methods provide a cost-effective opportunity to estimate model parameters using uncertain but abundant remotely-sensed observations of land and water allocated to crops (Maneta and Howitt, 2014). In this paper, we present and demonstrate a hydro-economic modeling framework that can be calibrated and applied over large regions by using recent advances in remote sensing and data assimilation methods to enable automatic model updates and calibration refinements. This recursive and stochastic process is of interest because (1) it permits calibration of model parameters with

frequent but noisy observations from satellite-based remote sensors that are available free-of-charge at global extents. This advance eliminates the cost of conducting expensive field surveys typically used for calibration, and it avoids biases introduced in calibration if producer surveys do not adequately represent regional practices. (2) The process permits refinement of model parameterization when new information becomes available without conducting a full batch (retrospective) calibration with the entire historical dataset. (3) In addition, the need to permanently store the historical dataset is eliminated. (4) This process blends information from old and new observations with the option of emphasizing the most recent measurements, making the model parameterization more relevant for current conditions. (5) Last, the process provides an automatic assessment of prediction uncertainty, thus avoiding the false sense of precision given by deterministic models. These innovations overcome current limitations of hydro-economic models and allow for the development of new insights into how farmers behave under resource and policy constraints. Herein, we demonstrate the implementation of the hydro-economic model and define its accuracy for hydrologic and agricultural systems in the State of Montana. These systems span a representative range of conditions in the western U.S., including extensive dryland agriculture that is particularly vulnerable to climate variability.

2. Model description

2.1. General approach

Our modeling package links an aggregated economic model of agricultural production operating at a seasonal scale, to a hydrologic model that simulates rainfall-runoff processes and water redistribution and availability in the regional streamflow network at daily time scales. The hydrologic model provides physical constraints on water availability and propagates the hydrologic impacts of agricultural activity and decision making to downstream users. The linked model is embedded in a stochastic data assimilation framework that facilitates adjustment of the economic model parameters when remote sensing observations of crop mix, land use allocation, yield, evapotranspiration, and other ancillary and hydrometric information become available (Figure 1). Once the model is calibrated, it can be used to simulate climatic and policy scenarios and make spatially-explicit predictions of the impacts of these scenarios on land and water allocation, crop yields, the opportunity cost of water, and on the hydrologic system. The data assimilation framework allows us to use observations with high uncertainty (typical of remote sensing observations) and incorporate this observational uncertainty in the probability distributions of economic model parameters. When the model is used for scenario analysis, parameter uncertainty is propagated to produce the probability distribution of the model predictions. Currently, only parameters and outputs from the economic component are treated as stochastic variables. For computational reasons, the hydrologic component and all hydroclimatic inputs to the economic component are deterministic.

2.2. Economic model of agriculture and farmer behavior

The backbone of the economic component is a nonlinear, constrained, optimization model calibrated to

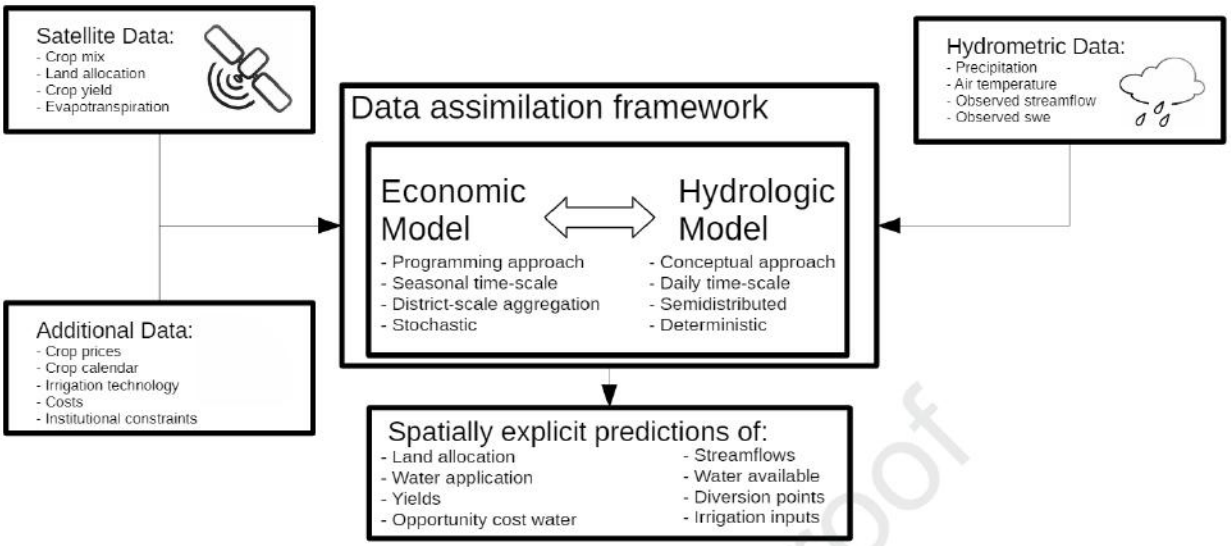

Figure 1: Overview of the hydro-economic modeling package. An economic model of agricultural production is linked to a spatially explicit hydrologic model and embedded in a stochastic data assimilation framework. The data assimilation framework adjusts the economic component parameters based on the ingestion of remote sensing observations of agricultural activity and other hydrometric and ancillary data. Once the model is calibrated, it can be used to predict probabilities of resource allocation under designed climate and policy scenarios.

in the assumption that producers allocate resources, in our case land and water, to maximize their net revenues subject to resource constraints:

$$\max_{x_{land,i},x_{water,i}} net = \sum_i \{p_i \pi_i \left(x_{land,i}, x_{water,i}; \mu_i, \beta_{land,i}, \beta_{water,i}, \rho_i, \delta_i\right) - c_{land,i} x_{land,i} - c_{water,i} x_{water,i}\}$$

$$\text{subject to:}$$

$$\sum_i x_{land,i} \leq \overline{L} \left[\overline{\lambda}_L\right]$$

$$\sum_i x_{water,i} \leq \overline{W} \left[\overline{\lambda}_W\right]$$

$$x_{land,i}, x_{water,i} \geq 0 \tag{1}$$

where net is net revenue, defined as revenue less the costs of land and water use; the index $i = 1, ..., I$ represents crops; $x_{land,i}, x_{water,i}$ represent land and water resource inputs for crop i, respectively; p_i is the price received for crop i; π_i is a production function that maps resource inputs to total production of crop i; and $c_{land,i}$, $c_{water,i}$ are the unit costs associated with land and water use to produce crop i. The parameters

the total land and water used for all crops in the region must be less than or equal to the total land $\overline{L}$ and water $\overline{W}$ available for cultivation and that resource allocation has to be non-negative. Note that total water available for cultivation refers to irrigation water, not precipitation. The total land and water available for cultivation may be constrained by physical limits (e.g., streamflow) or by policy or other institutional constraints (e.g., water rights or reservoir storage release policies).

Consistent with the recent economic literature on PMP (Mérel et al., 2011), we define the production function in Eq. (1) using a generalized constant elasticity of substitution (CES) functional form:

$$\pi_i = \mu_i \left[\beta_{land,i} x_{land,i}^{\rho_i} + \beta_{water,i} (x_{water,i} + x_{precip,i})^{\rho_i} \right]^{\frac{\delta_i}{\rho_i}} \tag{2}$$

A limitation of previous research in this area is that it has differentiated the production function in Eq. (2) for irrigated and non-irrigated crops, requiring independent calibration of each function (e.g. Maneta et al., 2009b). In this study, we streamline calibration by incorporating a production function that can handle irrigated and non-irrigated cases. To do so, we separate the total amount of water available to support crop growth into an exogenous component provided by natural sources like precipitation $x_{precip,i}$ (not controlled by the farmer), and an endogenous component provided by supplemental irrigation, $x_{water,i}$ (controlled by the farmer). Precipitation therefore acts as an offset to the total irrigation water applied to a crop and is not subject to the water availability constraint. This formulation also allows us to differentiate the costs of providing water for crop production, which differ depending on whether a year has relatively wet or dry conditions.

2.3. Hydrologic component

The hydrologic component provides water availability constraints to agricultural production. Precipitation is transformed into runoff using a gridded version of the *Hydrologiska Byråns Vattenbalansavdelning* (HBV) model (Bergstrom and Forsman, 1973; Bergstrom, 1995; Lindström et al., 1997). When runoff reaches the channel it is routed through the stream network using the Muskingum-Cunge method Cunge (1969). The HBV model and the Muskingum-Cunge method are well-known in the field of hydrology, and because of their parsimonious nature, reliability, robustness, and performance they have been widely applied in many regions of the world for hydrologic response analysis under climate change and drought (Driessen et al., 2010; Menzel and Bürger, 2002).

HBV is a precipitation-runoff model originally developed to assist in flood forecasting in Sweden (Bergstrom and Forsman, 1973). The hydrologic system is conceptualized as a cascade of four compartments: snowpack, soil, upper groundwater zone, and lower groundwater zone in each of the hydrologic response units (HRUs) in which the user may divide the region (Appendix Appendix A). Water outputs from the soil and groundwater compartments of each HRU are transformed into runoff by convolution with a triangular unit hydrograph. We implemented this particular application as a partially-gridded version of the original model. The model

aggregated (spatially-averaged) runoff response of the different subcatchments composing the study area. Water ponded on the surface of pixel k at time t available for infiltration and for the generation of runoff represents the integration of water input rates from snowmelt $Melt_{k,t}$, rainfall $Rain_{k,t}$ and supplemental irrigation $P^{irr}_{k(j),t}$ if pixel k is in the set of pixels designated to be irrigated from water source j,

$$Pond_{k,t} = Pond_{k,t-1} + (Melt_{k,t} + Rain_{k,t} + P^{irr}_{k(j),t})\Delta t - \Delta SM_{k,t} \tag{3}$$

Infiltration (described in Appendix A) increases the water storage in the soil ($\Delta SM_{k,t}$) at pixel k and is aggregated over all pixels k within subcatchment l. When water stored in the soil moisture compartment of subcatchment l reaches a threshold, the excess water generates output or percolates to the groundwater compartment. Outputs from the soil and groundwater compartments produce the integrated response of the subcatchment. A comprehensive description of our particular implementation of the model is provided in Appendix A. In total, the hydrologic model tracks four internal states in each of the subcatchments: snow water equivalent, soil water storage, water storage in the upper groundwater compartment, and water storage in the deep water compartment. The model has 12 parameters that can be potentially tuned. Details of the model structure and implementation are provided in Appendix A.

The runoff response of each subcatchment becomes lateral water contributions into the stream reach contained in the subcatchment. Lateral runoff and inflows from upstream subcatchments are routed through the river network using the Muskingum-Cunge model. The Muskingum model uses a two-parameter constitutive equation to relate storage (S) in a reach to its inflows (Q_{in}) and outflows (Q_{out}): $S = K\left[eQ_{in} + (1-e)Q_{out}\right]$, where K and e are the two function parameters. This constitutive relationship permits a mass balance equation for the reach as a function of streamflows and parameters. The Muskingum-Cunge method uses this relationship to develop a finite difference approximation of the 1D diffusion equation:

$$Q^{t+1}_j\left[K_j(1-e_j) + 0.5\Delta t\right] + Q^{t+1}_{j-1}\left[K_j e_j - 0.5\Delta t\right] \tag{4}$$

$$= Q^{t}_j\left[K_j(1-e_j) - 0.5\Delta t\right] + Q^{t}_{j-1}\left[K_j e_j + 0.5\Delta t\right] \tag{5}$$

$$+ (q^{t+1}_j - q^{irr}_{j,i,t+1})\left[K_j(1-e_j) + 0.5\Delta t\right] \tag{6}$$

Full details on the Muskingum-Cunge algorithm and its implementation are provided in Appendix A.

2.4. Model coupling

The hydrologic component of the model operates deterministically at daily time steps and at variable spatial resolutions defined by the size of the HRUs. On the other hand, the economic component operates stochastically at seasonal time steps and at spatial resolutions defined by counties, districts, or regions that may or may not be coincident with the HRUs. To couple the two components, relevant information generated

resolution of the receiving component, as described in this section. At the beginning of each simulated year, the economic component is run for each economic unit within the domain and the simulated probabilistic ensembles of land $\mathbf{x}_{land,i}$ and irrigation water $\mathbf{x}_{water,i}$ allocated to each crop i for the growing season are determined. The ensemble average of seasonal water allocations $\mathbb{E}[\mathbf{x}_{water,i}]$ are temporally and spatially disaggregated and combined with information on irrigation and conveyance efficiencies to obtain expected daily diversion volumes from the hydrologic network and pixel-level water application rates.

The temporal disaggregation of simulated seasonal water allocation for each crop i $\mathbb{E}[\mathbf{x}_{water,i}]$ to daily water diversion rates from its source node j in the hydrologic network is achieved by redistributing the seasonal water allocation to daily amounts over the growing season according to a fractional weight coefficient $\omega_{i,t+1}$ that reflects the growth stage of the crop at a given day:

$$q^{irr}_{j,i,t+1} = \frac{\mathbb{E}[\mathbf{x}_{water,i}] * \omega_{i,t+1}}{I_{eff_i}} \tag{7}$$

where:

$$\omega_{i,t+1} = \frac{Kc_{i,t+1}}{\sum_t Kc_{i,t+1}}, \tag{8}$$

where $q^{irr}_{j,i,t+1}$ is the water volume diverted for irrigation from river node j for crop i at day $t+1$; I_{eff_i} is an irrigation and conveyance efficiency factor for crop i; and $\omega_{i,t+1}$ is a weight factor that represents the fraction of the total crop water requirement that correspond to day $t+1$. Factor $\omega_{i,t+1}$ is a function of crop coefficients Kc that vary through the season from plant emergence to termination and reflect crop water requirements at a given stage relative to the water requirement of a fully developed reference crop. We use crop coefficients and growth curve charts recommended by the U.S Bureau of Reclamation for the Pacific Northwest Region (Agrimet program[2]). Computed daily diverted volumes enter the hydrologic model through Eq. 4.

Daily diverted water from each source node $q^{irr}_{j,i,t+1}$ is subsequently spatially disaggregated and distributed to pixels identified as irrigated agriculture within the economic unit supplied by the diversion node. Application rates in each irrigated pixel are obtained by dividing daily diverted volumes by the irrigated area in the economic unit:

$$P^{irr}_{k(j),t+1} = \frac{\sum_i q^{irr}_{j,i,t+1}}{N_k \Delta x^2}, \tag{9}$$

where $P^{irr}_{k(j),t}$ is the supplemental irrigation applied at time t on pixel k from the set of pixels classified as irrigated agriculture within the economic unit associated with diversion point j; N_k is the total number of pixels classified as irrigated agriculture within the economic units; and Δx^2 is the pixel area. Computed daily water application rates (P^{irr}) enter the hydrologic model as supplemental irrigation in Eq. 3. Since

[2] https://www.usbr.gov/pn/agrimet/cropcurves/crop_curves.html

the model spatial resolution is typically too coarse to resolve individual crops, irrigation is applied uniformly over all pixels k designed as irrigated crops within the corresponding economic unit

3. Calibration of the economic component

3.1. Positive Mathematical Programming

The PMP approach assumes that farmers allocate limited land and water resources with the objective of maximizing net revenues, and thus past observations of land and water use by crop $(\overline{x}_{land,i}, \overline{x}_{water,i})$ are solutions to the problem in Eq. (1). During calibration, Eq. (1) is modified to constrain the maximization problem to the observed levels of land and water allocation:

$$\begin{aligned}
\max_{x_{land,i}, x_{water,i}} net = & \sum_i \left\{ p_i \pi_i \left(x_{land,i}, x_{water,i}; \mu_i, \beta_{land,i}, \beta_{water,i}, \rho_i, \delta_i \right) - c_{land,i} x_{land,i} - c_{water,i} x_{water,i} \right\} \\
& \text{subject to:} \\
& \sum_i x_{land,i} \leq \overline{L} \left[\overline{\lambda}_{fsl} \right] \\
& x_{land,i} = \overline{x}_{land,i} \left[\lambda_{land,i} \right] \\
& x_{water,i} = \overline{x}_{water,i} \left[\lambda_{water,i} \right] \\
& x_{land,i}, x_{water,i} \geq 0
\end{aligned} \tag{10}$$

Equation (10) contains seven parameters per crop: five production function parameters $\mu_i, \beta_{i,land}, \beta_{i,water}, \rho_i, \delta_i$, and two Lagrange multipliers associated with the observed land and water-use constraints $\lambda_{i,land}, \lambda_{i,water}$, for a total of 7 unknown parameters to be calibrated based on observed decision making. An additional parameter, $\overline{\lambda_{fsl}} > 0$ associated with the land resource constraint also needs to be calibrated. This parameter represents the shadow value for the total amount of land available for crop production. The PMP methodology builds the system of optimality conditions associated with Eq. (10), however instead of solving the maximization problem to find optimal land and water resource allocation, the method fixes these at the observed allocation levels and solves the system of optimality conditions for the model parameters. In essence, the PMP methodology finds the parameters that produce a response surface (net revenue function) that is maximum at the observed resource allocation levels $(\overline{x}_{land,i}, \overline{x}_{water,i})$. Eq. 10 is differentiable and traditionally solved using nonlinear programming methods. Necessary and sufficient optimality conditions are given by the first order derivatives of Eq. 10 with respect to $x_{land,i}$ and $x_{water,i}$, the Karush-Kuhn-Tucker conditions to enforce constraints, and a few additional constraints to ensure the solution to the maximization problem exists and is unique. A programming solution embedding the optimality conditions for Eq. 10, proposed by Mérel et al. (2011) and used in this study, is provided in Appendix B. Additionally, we follow

between modeled expenditures on inputs and expenditures implied by the observed use of inputs. This deterministic program of optimality conditions can be arranged such as the observed quantities are grouped on the left hand side (LHS), and the quantities that depend on model parameters (functions of model parameters) are grouped on the right hand side (RHS):

$$
\begin{array}{ccc}
-p_i\,\overline{\pi}_i\,\overline{\pi}_{W,i} & = & \left(c_{land,i}+\lambda_{land,i}+\overline{\lambda}_{fsl}\right)\overline{x}_{land,i}-p_i\,\overline{\pi}_i\,\delta_i \\
p_i\,\overline{\pi}_i\,\overline{\pi}_{W,i} & = & \left(c_{water,i}+\lambda_{water,i}\right)\overline{x}^{*}_{water,i} \\
\overline{\eta_i} & = & \frac{\delta_i}{1-\delta_i}\left\{1-\frac{\frac{b_i}{\delta_i(1-\delta_i)}}{\sum_i\left[\frac{b_i}{\delta_i(1-\delta_i)}+\frac{\sigma_i b_i \overline{\pi}_{W,i}}{\delta_i\left(\delta_i-\overline{\pi}_{W,i}\right)}\right]}\right\},\quad b_i=\frac{(\overline{x}_{land,i})^2}{p_i\,\overline{\pi}_i} \\
\overline{\pi}_{W,i} & = & \delta_i\left(\frac{\beta_{water,i}(\overline{x}_{water,i})^{*\rho_i}}{\beta_{land,i}(\overline{x}_{land,i})^{\rho_i}+\beta_{water,i}(\overline{x}_{water,i})^{*\rho_i}}\right) \\
\overline{\pi_i} & = & \mu_i\left[\beta_{land,i}(\overline{x}_{land,i})^{\rho_i}+\beta_{water,i}(\overline{x}_{water,i})^{*\rho_i}\right]^{\frac{\delta_i}{\rho_i}} \\
\sum_{i=0}^{I}\left(2\,\overline{x}_{land,i}\,p_i\,\overline{\pi}_i^{m}\,\overline{\pi}_{W,i}^{m}\right) & = & \sum_{i=0}^{I}\left[-2(c_{land,i}+\overline{\lambda}_{fsl})\left(\overline{x}_{land,i}\right)^2+2\,\overline{x}_{land,i}\,p_i\,\overline{\pi}_i\,\delta_i\right] \\
1 & = & \beta_{land_i}+\beta_{water_i}
\end{array}
\qquad (11)
$$

$\underbrace{\qquad\qquad}_{LHS}$ $\qquad$ $\underbrace{\qquad\qquad\qquad\qquad\qquad\qquad\qquad\qquad}_{RHS}$

During calibration the standard PMP solves this nonlinear program for the model parameters using a standard root-finding algorithm.

3.2. Stochastic Recursive Parameter Estimation

In the stochastic approach, we embed Eq. (11) within a stochastic data assimilation framework that permits the recursive calibration of the model parameters while taking into account the impact of observational errors. The basic idea of the algorithm is to generate an ensemble of LHS quantities any time new observations are available by drawing samples from the probability distribution of the observations. This LHS ensemble is compared with an ensemble of RHS quantities. The ensemble of RHS quantities is generated by running the RHS functions using random samples from a model parameter distribution. The difference between LHS and RHS is called the innovation, and is a diagnostic of optimality. Over time, as more observations are used, the data assimilation algorithm adjusts (updates) the model parameter distribution to values that result in an innovation ensemble with mean zero. This condition indicates that the parameter distribution satisfies the optimality conditions in the stochastic sense. The key in this process is the parameter update algorithm, which is presented in section 3.2.4. A schematic overview of the algorithm is shown in Figure 2.

Maneta and Howitt (2014) describe a discrete Monte Carlo recursive Bayesian estimator that permits to update the parameters as new observations become available at time k. In our application, time k represents a year because observations of agricultural activity are available yearly. The proposed methodology has three important advantages: 1) its probabilistic nature permits to integrate noisy observations in the parameter estimation process, making possible the use of remote sensing retrievals of agricultural activity for model

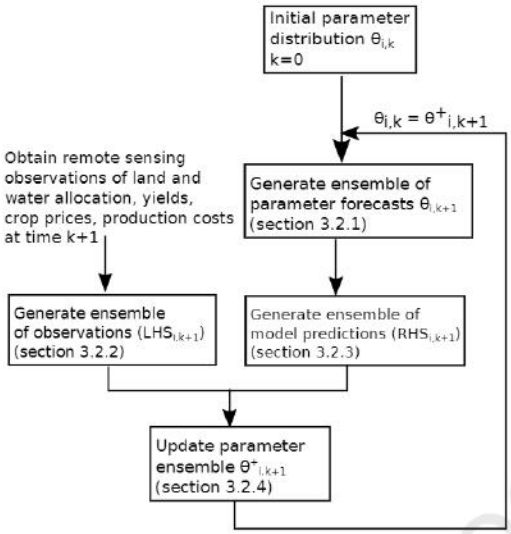

Figure 2: Schematic overview of the stochastic recursive parameter estimation of the positive mathematical programming (PMP) methodology

calibration; 2) it provides a posterior parameter distribution that reflects the quality of the information used for calibration; and 3) it integrates new and old information when new observations are available without having to store or retrieve the old history of observations.

The equations of the estimator are based on the ensemble Kalman Filter, enKF (Evensen, 1994), where the probability distribution of parameters, inputs and observations are represented by a Monte Carlo sample. The exception is parameter ρ_i, a function of σ_i, which controls the elasticity of substitution between land and water. This parameter is fixed at a value $\rho_i = \frac{\sigma_i - 1}{\sigma_i}$, with σ_i values typically in the range of 0.1 to 0.6, which represents limited substitution between these two resources. The reason for fixing this parameter is that elasticity of substitution has been found to be insensitive to aggregated observations and requires more detailed experimental data for its identification. Therefore, our approach stochastically tracks seven parameters, six parameters that need to be calibrated for each crop, and one unit-level resource constraint parameter ($\overline{\lambda}_{fsl}$). Specifically, the probability distribution of the model parameters $\boldsymbol{\theta} = \{\boldsymbol{\mu}, \boldsymbol{\beta}_{land}, \boldsymbol{\beta}_{water}, \boldsymbol{\delta}, \boldsymbol{\lambda}_{land}, \boldsymbol{\lambda}_{water}, \overline{\lambda}_{fsl}\}$ is represented by a random ensemble of M members $m = 1, ..., M$ of $\boldsymbol{\theta}$. Except for $\overline{\lambda}_{fsl}$, the unit-level parameter, each bold parameter in the $\boldsymbol{\theta}$ set is an array with rows representing parameter values for each crop grown in a given economic unit (e.g. county, irrigation district) and each column is an individual member of the ensemble. The parameters of the generalized CES production function must satisfy the following constraints: $\boldsymbol{\mu} > 0$, $\boldsymbol{\beta}_{land} > 0$, $\boldsymbol{\beta}_{water} > 0$, $0 < \boldsymbol{\delta} < 1$, and $\overline{\lambda}_{fsl} \geq 0$. The parameters $\boldsymbol{\lambda}_{land}$ and $\boldsymbol{\lambda}_{water}$ are unrestricted. A positive value for the λ parameters reflects an unobserved cost associated with the use of an input, whereas a negative value reflects an unobserved benefit, as described by Mérel et al. (2014).

3.2.1. Prior parameter distribution (parameter forecasts)

To set the filter equations, we treat model parameters as if they were the system states of the standard enKF. The evolution of parameters (forecasts) from period k to $k+1$ (periods when observations become available, typically yearly) is produced by adding a random perturbation to each member of the ensemble. The addition of artificial noise to each ensemble member to simulate time dynamics results in an overdispersed ensemble that overestimates the parameter variance (West, 1993). This is because the intrinsic variance of the ensemble is compounded by the noise added to each member to perform the random walk. Liu and West (West, 1993) show that this can be corrected by using perturbations that are proportional to the ensemble variance by a number h slightly smaller than one, and shrinking the ensemble toward its mean by a factor $a = \sqrt{1-h}$. For a given crop i, the dynamics of members of the parameter ensemble with shrinkage is:

$$\underbrace{\begin{bmatrix} \beta^m_{land,i,k+1} \\ \beta^m_{water,i,k+1} \\ \mu^m_{i,k+1} \\ \delta^m_{i,k+1} \\ \lambda^m_{land,i,k+1} \\ \lambda^m_{water,i,k+1} \\ \overline{\lambda}^m_{fsl,k+1} \end{bmatrix}}_{\boldsymbol{\theta}^m_{i,k+1}} = a \begin{bmatrix} 0 \\ 0 \\ \mu^{m+}_{i,k} \\ \delta^{m+}_{i,k} \\ \lambda^{m+}_{land,i,k} \\ \lambda^{m+}_{water,i,k} \\ \overline{\lambda}^{m+}_{fsl,k} \end{bmatrix} + (1-a) \begin{bmatrix} 0 \\ 0 \\ \mathbb{E}[\boldsymbol{\mu}^+_{i,k}] \\ \mathbb{E}[\boldsymbol{\delta}^+_{i,k}] \\ \mathbb{E}[\boldsymbol{\lambda}^+_{land,i,k}] \\ \mathbb{E}[\boldsymbol{\lambda}^+_{water,i,k}] \\ \mathbb{E}[\overline{\boldsymbol{\lambda}}^+_{fsl,k}] \end{bmatrix} + \begin{bmatrix} \zeta^{\beta_{land}}_{i,k} \\ \zeta^{\beta_{water}}_{i,k} \\ \zeta^{\mu}_{i,k} \\ \zeta^{\delta}_{i,k} \\ \zeta^{\lambda_{land}}_{i,k} \\ \zeta^{\lambda_{water}}_{i,k} \\ \zeta^{\overline{\lambda}_{fsl}}_{k} \end{bmatrix} +, \quad \begin{array}{l} \zeta^{\beta_{land}}_{i,k} \sim \mathcal{B}\left(\hat{a}_i(\boldsymbol{\beta}^+_{land,k}), \hat{b}_i(\boldsymbol{\beta}^+_{land,k})\right) \\ \zeta^{\beta_{water}}_{i,k} \sim \mathcal{B}\left(\hat{a}_i(\boldsymbol{\beta}^+_{water,k}), \hat{b}_i\boldsymbol{\beta}^+_{water,k})\right) \\ \zeta^{\mu}_{i,k} \sim \mathcal{N}\left(0, h^2\mathbb{V}[\mu^+_{i,k}] + \mathbb{V}^*_{\mu,k}\right) \\ \zeta^{\delta}_{i,k} \sim \mathcal{N}\left(0, h^2\mathbb{V}[\delta^+_{i,k}] + \mathbb{V}^*_{\delta,k}\right) \\ \zeta^{\lambda_{land}}_{i,k} \sim \mathcal{N}\left(0, h^2\mathbb{V}[\lambda^+_{land,i,k}] + \mathbb{V}^*_{\lambda_{land},k}\right) \\ \zeta^{\lambda_{water}}_{i,k} \sim \mathcal{N}\left(0, h^2\mathbb{V}[\lambda^+_{water,i,k}] + \mathbb{V}^*_{\lambda_{water},k}\right) \\ \zeta^{\overline{\lambda}_{fsl}}_{k} \sim \mathcal{N}\left(0, h^2\mathbb{V}[\overline{\lambda}^+_{fsl,k}] + \mathbb{V}^*_{\overline{\lambda}_{fsl},k}\right) \end{array}, \tag{12}$$

where superscript m over a a parameter indicates it is the mth ensemble member at the time indicated by the subscript k, and superscript $+$ indicates the parameter is corrected (posterior) after data assimilation at time k (see below); a and h are shrinkage and variance smoothing parameters, respectively; $\mathbb{E}[\cdot]$ is the expectation operator of the parameter ensemble (i.e. ensemble average for the given parameter and crop), operator $\mathbb{V}[\cdot]$ is the parameter ensemble variance and $\mathbb{V}^*_{\cdot}$ is a parameter-level background variance that represents the parameter forecast processes noise. $\mathbb{V}^*_{\cdot,k}$ and h are important tuning parameter that permits to control filter divergence and collapse. Parameters $\mu, \delta, \lambda_{land}, \lambda_{water}$ and $\overline{\lambda}_{fsl}$ are sampled using normally distributed noise, however the β parameters are bound to values in the range [0,1]. To sample the distribution of these parameters at $k+1$ we used a Beta distribution with two shape parameters, $\hat{a}, \hat{b}$ centered at each ensemble member. The parameters that center the distribution at each member are determined using the method of moments from the mean and the variance of each individual ensemble member:

$$\begin{aligned} \hat{a}_i(\beta_{\cdot}) &= <\boldsymbol{\beta}^m_{\cdot,i}> \left(\frac{<\boldsymbol{\beta}^m_{\cdot,i}>(1-<\boldsymbol{\beta}^m_{\cdot,i}>)}{\mathbb{V}[\beta^+_{\cdot,i,k}] + \mathbb{V}^*_{\beta_{\cdot},k}} - 1 \right) \\ \hat{b}_i(\boldsymbol{\beta}_{\cdot}) &= (1-<\boldsymbol{\beta}^m_{\cdot,i}>)\hat{a}_i(\beta_{\cdot,i}), \end{aligned} \tag{13}$$

and $< \beta^m_{\cdot,i} >$ is the mean of the kernel locations and :

$$< \beta^m_{\cdot,i} >= a\beta^{m+}_{\cdot,i,k} + (1-a)\mathbb{E}[\beta^+_{\cdot,i,k}] \tag{14}$$

3.2.2. Generation of the observation (LHS) ensemble

Uncertainty in remote sensing observations of agricultural activity (land and water allocations, crop yield and yield elasticity) as well as uncertainty in additional ancillary information (crop supply elasticity, crop price, cost of operating land and cost of water) obtained at time $k+1$ is represented by an ensemble with M observations of replicates obtained by sampling from a Normal distribution centered at the observation:

$$\begin{aligned}
\overline{x}^m_{land,i,k+1} &= \overline{x}_{land,i} + \nu^m_{land,i,k+1}, \qquad \nu^m_{land,i,k+1} \sim \mathcal{N}\left(0, R^{x_{land}}_{k+1}\right) \\
\overline{x}^m_{water,i,k+1} &= \overline{x}_{water,i} + \nu^m_{water,i,k+1}, \qquad \nu^m_{water,i,k+1} \sim \mathcal{N}\left(0, R^{x_{water}}_{k+1}\right) \\
\overline{\pi}^m_{W,i,k+1} &= \overline{\pi}_{W,i,k+1} + \nu^m_{\pi_W,i,k+1}, \qquad \nu^m_{\pi_W,i,k+1} \sim \mathcal{N}\left(0, R^{\pi_W}_{k+1}\right) \\
\overline{\pi}^m_{i,k+1} &= \overline{\pi}_{i,k+1} + \nu^m_{\pi,i,k+1}, \qquad \nu^m_{\pi,i,k+1} \sim \mathcal{N}\left(0, R^{\pi}_{k+1}\right) \\
\overline{\eta}^m_{i,k+1} &= \overline{\eta}_{i,k+1} + \nu^m_{\eta,i,k+1}, \qquad \nu^m_{\eta,i,k+1} \sim \mathcal{N}\left(0, R^{\eta}_{k+1}\right) \\
p^m_{i,k+1} &= p_{i,k+1} + \nu^m_{p,i,k+1}, \qquad \nu^m_{p,i,k+1} \sim \mathcal{N}\left(0, R^{p}_{k+1}\right) \\
c^m_{land,i,k+1} &= c_{land,i} + \nu^m_{cland,i,k+1}, \qquad \nu^m_{cland,i,k+1} \sim \mathcal{N}\left(0, R^{c_{land}}_{k+1}\right) \\
c^m_{water,i,k+1} &= c_{water,i} + \nu^m_{cwater,i,k+1}, \qquad \nu^m_{cwater,i,k+1} \sim \mathcal{N}\left(0, R^{c_{water}}_{k+1}\right),
\end{aligned} \tag{15}$$

where $\overline{x}^m_{land,i}, \overline{x}^m_{water,i}, \overline{\pi}_{W,i}, \overline{\pi}_{W,i}$, and $\overline{\eta}_i$, are observations of land and water used by crops, elasticity of production to water inputs, crop production, and elasticity of production to crop prices, respectively. Observations are scaled into a dimensionless quantity (see section 3.3).

Using these observation replicates, individual LHS_i ensemble members of the stochastic system of optimality condtions are produced:

$$LHS^m_{i,k+1} = \begin{bmatrix}
-p^m_i\,\overline{\pi}^m_i\,\overline{\pi}^m_{W,i} & (1) \\
p^m_i\,\overline{\pi}^m_i\,\overline{\pi}^m_{W,i} & (2) \\
\overline{\eta_i}^m & (3) \\
\overline{\pi}^m_{W,i} & (4) \\
\overline{\pi_i}^m & (5) \\
\sum_{i=0}^{I}\left(2\,\overline{x}^m_{land,i}\,p^m_i\,\overline{\pi}^m_i\,\overline{\pi}^m_{W,i}\right) & (6) \\
1 & (7) \\
0 & (8) \\
0 & (9)
\end{bmatrix}_{k+1} \tag{16}$$

where the first two elements are part of the calculation of the marginal costs of production, the next two

retrieved by remote sensing algorithms), respectively, the fifth element is the observations of crop production and the last three elements are the left hand side of three constraints to facilitate sampling β parameters such as $\beta_{land,i} + \beta_{water,i} = 1, \beta_{\cdot,i} \geq 0$. Since all inputs are normalized, the β parameters represent the fraction of production shared by the corresponding input. The constraints on the β parameters form a convex sum of inputs that ensure that the production function outputs are always within the range of historical observations.

3.2.3. Generation of the model prediction (RHS) ensemble

The $RHS(\theta_{k+1})$ ensemble is a function of model parameters $\theta_{i,k+1}$. Using parameter and input replicates, the right hand side equations are used to producean ensemble of model prediction counterparts to the observations in $LHS_{i,k+1}$:

$$RHS(\theta^m_{i,k+1}) = \begin{bmatrix} \left(c^m_{land,i} + \lambda^m_{land,i} + \overline{\lambda}^m_{fsl}\right) \overline{x}^m_{land,i} - p^m_i \, \overline{\pi}^m_i \, \delta^m_i & (1) \\ \left(c^m_{water,i} + \lambda^m_{water,i}\right) \overline{x}^{*m}_{water,i} & (2) \\ \frac{\delta^m_i}{1-\delta^m_i} \left\{ 1 - \frac{\frac{b_i}{\delta^m_i(1-\delta^m_i)}}{\sum_i \left[\frac{b_i}{\delta^m_i(1-\delta^m_i)} + \frac{\sigma^m_i b_i \overline{\pi}^m_{W,i}}{\delta^m_i \left(\delta^m_i - \overline{\pi}^m_{W,i}\right)} \right]} \right\}, \quad b_i = \frac{(\overline{x}^m_{land,i})^2}{p^m_i \, \overline{\pi}^m_i} & (3) \\ \delta^m_i \left(\frac{\beta^m_{water,i} (\overline{x}^m_{water,i})^{*\rho_i}}{\beta^m_{land,i} (\overline{x}^m_{land,i})^{\rho_i} + \beta^m_{water,i} (\overline{x}^m_{water,i})^{*\rho_i}} \right) & (4) \\ \mu^m_i \left[\beta^m_{land,i} (\overline{x}^m_{land,i})^{\rho_i} + \beta^m_{water,i} (\overline{x}^m_{water,i})^{*\rho_i} \right]^{\frac{\delta^m_i}{\rho_i}} & (5) \\ \sum_{i=0}^{I} \left[-2(c^m_{land,i} + \overline{\lambda}^m_{fsl}) \, (\overline{x}^m_{land,i})^2 + 2 \, \overline{x}^m_{land,i} \, p^m_i \, \overline{\pi}^m_i \, \delta^m_i \right] & (6) \\ \beta^m_{land_i} + \beta^m_{water_i} & (7) \\ \beta^m_{land_i} - |\beta^m_{land_i}| & (8) \\ \beta^m_{water_i} - |\beta^m_{water_i}| & (9) \end{bmatrix}_{k+1} \tag{17}$$

The first two elements of LHS^m_i and RHS^m_i represent the difference between marginal costs of production and marginal revenues with respect to land and water. Marginal costs and marginal revenues are equal at the optimal point. The next two elements of $RHS^m_{i,k+1}$ are model predictions of production elasticity to crop price and production elasticity to crop water use, respectively; the fifth element is the observation of crop production. The last three elements of LHS^m_i and RHS^m_i are constraints to facilitate sampling β parameters within the unit simplex, such as $1 = \beta_{land,i} + \beta_{water,i}, \beta_{\cdot,i} \geq 0$. The last two constraints are the non-negativity conditions. Non-negative β samples only occur if the difference between the sample and its absolute is zero, which is the condition expressed by the last two equations.

3.2.4. Assimilation equations - Posterior parameter distribution

Assimilation of new observations obtained at time $k+1$ to correct each member m of the parameter ensemble is achieved using the update equations of the enKF:

$$\theta^{m+}_{i,k+1} = \theta^m_{i,k+1} + K_{k+1} \left(LHS^m_{i,k+1} - RHS(\theta^m_{i,k+1}) \right) \tag{18}$$

where $\theta^{m+}_{i,k+1}$ is the corrected (posterior) mth member of the model parameters, K_{k+1} is the Kalman gain matrix that corrects the parameter trajectories; $LHS^{m}_{i,k+1}$ is the mth member of the ensemble of replicates of the left hand side of the system of optimality conditions, which holds observation and other derived quantities; $RHS(\theta^{m}_{i,k+1})$ is the mth member of the ensemble of replicates of the right hand side of the optimality conditions, which is a function of model parameters, and holds predictions of the LHS; $\boldsymbol{C}^{\theta,LHS}_{k+1}$ is the cross-covariance between the parameter ensemble and the RHS ensemble, $\boldsymbol{C}^{LHS}_{k+1}$ is the covariance of the LHS ensemble and $\boldsymbol{C}^{RHS}_{k+1}$ is the covariance of the RHS ensemble.

The quantity between brackets in the top equation of (18) is the innovation and holds the model prediction errors. A property of Kalman filters is that when they are properly tuned, the ensemble of parameters produce a sequence of innovations that is normally distributed with zero mean. Since LHS and RHS represent the left and right hand sides of the optimality conditions, Eq. 18 is in effect solving the maximization problem posed in Eq. 1. The variance of the innovation is the total variance of the process associated with observation and parameter uncertainty.

3.3. Scaling observations and inputs

If the β parameters are considered dimensionless share quantities, the constant elasticity of substitution production function specified in Eq. (2) is dimensionally inconsistent and its results are not interpretable in terms of processes unless inputs are scaled and transformed to dimensionless quantities. For a particular season, the information needed to correct the model parameters for an economic unit include observations of land ($x^{obs}_{land,i}$, ha) and water ($x^{obs}_{water,i}$ mm ha^{-1}) used by crop i, crop price (p^{obs}_{i}, \$t^{-1}), the typical cost of cultivating crop i per unit of land (c^{obs}_{land} \$ha^{-1}), the cost of applying a unit of water including fees, transportation, application costs, etc (c^{obs}_{water} \$/(mm ha), average crop yield over the economic unit (y^{obs}_{i}, t ha^{-1}), the elasticity of production to water (π^{obs}_{Wi}, dimensionless), and the elasticity of production to crop prices (η^{obs}_{i}, dimensionless).

The dimensionless observed quantities used in the data assimilation and parameter correction process are

obtained by applying the following transformations:

$$
\begin{aligned}
\overline{x}_{land,i} &= \frac{x^{obs}_{land,i}}{x^{ref}_{land,i}} \\
\overline{x}_{water,i} &= \frac{x^{obs}_{water,i}}{ET^{ref}_{i} * x^{ref}_{land,i}} \\
\overline{x}_{precip,i} &= \frac{x^{est}_{precip,i}}{ET^{ref}_{i}} \\
\overline{\pi}_{i} &= \frac{y^{obs}_{i} x^{obs}_{land,i}}{y^{ref}_{i} x^{ref}_{land,i}} \\
p_{i} &= \frac{p^{obs}_{i}}{p^{ref}_{i}} \\
c_{land,i} &= \frac{c^{obs}_{land,i}}{p^{ref}_{i} y^{ref}_{i}} \\
c_{water,i} &= c^{obs}_{water,i} \frac{ET^{ref}_{i}}{p^{ref}_{i} y^{ref}_{i}},
\end{aligned}
\tag{19}
$$

where y^{obs}_{i} is the mean observed yield in the economic unit ($\mathrm{kg\,ha^{-1}}$), $x^{est}_{precip,i}$ is the estimated or expected crop water use from natural water sources (e.g. from precipitation) in mm, and $x^{ref}_{land,i}$ in ha, ET^{ref}_{i} in mm, p^{ref}_{i} in $\$\mathrm{kg^{-1}}$ and y^{ref}_{i} in $\mathrm{kg\,ha^{-1}}$ are long term mean land, used water, price and yield observations used as reference scaling quantities for crop i. Note that the observed cost of water per unit volume ($c^{obs}_{water,i}$) only applies to artificial irrigation but is normalized using total crop evapotranspiration (ET^{ref}_{i}) because it is what is retrieved by remote sensing products. This normalization works because $c^{obs}_{water,i}$ is constant regardless of the water volume used by crops and ET^{ref}_{i} just serves the role of a normalization factor.

Elasticity to water and prices measures how responsive their production is to used water and crop prices and is defined as a percent change in production over a percent change in used water or crop price. Defining $\pi^{obs}_{i} = y^{obs}_{i} x^{obs}_{land,i}$, elasticities can be calculated from observations as:

$$
\overline{\pi}_{W,i} = \frac{\Delta\pi^{obs}_{i}/\pi^{obs}_{i}}{\Delta x^{obs}_{water,i}/x^{obs}_{water,i}} = \frac{d\log\pi^{obs}_{i}}{d\log x^{obs}_{water,i}} \tag{20}
$$

$$
\overline{\eta}_{i} = \frac{\Delta\pi^{obs}_{i}/\pi^{obs}_{i}}{\Delta p^{obs}_{i}/p^{obs}_{i}} = \frac{d\log\pi^{obs}_{i}}{d\log p^{obs}_{i}} \tag{21}
$$

Elasticities are typically considered constant over a period of time and they can be obtained as the least square regression slope between the logarithm of production and the logarithm of water used or the logarithm of crop prices over the considered period. We calculate the production elasticity to water, $\overline{\pi}_{W,i}$ in our study area empirically using (20). We constructed our crop-specific supply elasticity using results from a series of previous studies summarized in Appendix Appendix C. In addition, we supplemented published supply elasticity estimates with our own calculation from (21) applied using annual county-level production

combined with published values based on the temporal recency and geographical proximity of the studies, and based on expert judgment.

3.4. Economic component at simulation time

The posterior parameter distribution obtained after the most recent assimilation step K is used in the production and cost functions of the net revenue equation (1). For each member in the parameter ensemble, the maximization problem is solved, this time for land and water allocation under any simulation scenario represented by different crop prices, production costs, and land and water constraints:

$$\begin{aligned}
\max_{x^m_{land,i}, x^m_{water,i} \geq 0} net^m = & \\
& \sum_i \left\{ p_i \pi_i^m \left(x_{land,1}, x_{water,i} + x_{precip,i}; \mu^{m+}_{i,K}, \beta^{m+}_{land,i,K}, \beta^{m+}_{water,i,K}, \rho_i, \delta^{m+}_{i,K} \right) \right. \\
& - \left(c_{land,i} + \lambda^{m+}_{land,i,K} + \overline{\lambda}^{m+}_{fsl,K} \right) x^m_{land,i} \\
& \left. - \left(c_{water,i} + \lambda^{m+}_{water,i,K} \right) x^m_{water,i} \right\} \\
\text{subject to} \quad & \sum_i x^m_{land,i} \leq \overline{L} \left[\overline{\lambda}^m_{land} \right] \\
& \sum_i x^m_{water,i} \leq \overline{W} \left[\overline{\lambda}^m_{water} \right]
\end{aligned} \tag{22}$$

Maximization of equation (22) for each member m of the parameter ensemble generates a result ensemble that represents the probability distribution of land and water allocated to each crop i as well as an ensemble of the Lagrange multipliers $\overline{\lambda}^m_{land}$ and $\overline{\lambda}^m_{water}$ associated with total land $\overline{L}$ and water $\overline{W}$ resource constraints imposed by physical availability or policy. Lagrange multipliers represent the opportunity cost associated with not having an additional unit of land or water and therefore can be interpreted as a metric of the value of land and water. Additionally, solving equation (22) also produces the probability distribution of estimated crop production, and of the probability distribution of production elasticity of supply and production elasticity of water inputs.

4. Application to Montana

We demonstrate the application of the model at regional scales in the state of Montana, located in the intermountain Pacific northwest of the United States (inset of Figure 3). The study region extends beyond the boundaries of the state to include the headwaters of basins that drain into the state, covering an area of 464,800 km^2. The state has a longitudinal topographic and climatic gradient, from the steep and relatively wet Rocky Mountain western region toward the flatter and significantly drier eastern portions of the state, which are part of the US northern great plains region. The US continental divide runs roughly north to south along the west quarter of the state. About 25% of Montana drains to the Pacific Ocean (Clark Fork River

River basin) drains to the Gulf of Mexico. Annual precipitation inputs range from over 1000 $\mathrm{mm\,yr^{-1}}$ in the mountain regions of the west and gradually decline to about 200 $\mathrm{mm\,yr^{-1}}$ in eastern Montana. The western part of the state also shows less continentality, with relatively warmer temperatures in the winter and cooler temperatures in the summer than the eastern portion of the state.

Other than the ecosystem, the largest water user in the state is agriculture. Agriculture is also the leading industry in the state. Despite its economic importance, agriculture is poorly diversified and dominated in terms of production and planted area by alfalfa, wheat, and barley. Montana is a major producer of wheat and barley in the US and contributes to the country's food security. Irrigation is common along streams and in the western parts of the state, however rainfed production is dominant and very vulnerable to drought in the drier central and eastern parts of the state. Irrigated area has been growing substantially in the state in recent decades and has contributed to increasing production and reduction in economic risk. Surface water is the primary source for irrigation, including within irrigation districts, and so far significant groundwater depletion due to agricultural extraction is only limited to a few localized watersheds ((Whitlock et al., 2017, p. 120)).

4.1. Implementation of hydrologic component

The representation of the hydrologic system in the the study region is shown in Figure 3. The figure shows the representative elementary watersheds (REWs) that compose the domain, the nodes that define their outlets, and the links (stream reaches) that connect them. We used the GTOPO30 digital elevation model (DEM) produced by the USGS at 1Km resolution to determine the regional drainage network and partition the domain into REWs using GIS procedures. We used the location of active National Water Information System streamflow gauges as the initial set of nodes to partition the landscape into REWS and then further densified the network with additional nodes until we achieved sufficient spatial detail. The densification was done by allocating nodes in pixels having contributing areas larger than a specified threshold. The minimum contributing area for a REW was selected such that the total number and sizes of REWS was considered adequate to resolve the spatial variability of streamflows. The final domain contains over 300 REWS with typical sizes around 1400 $\mathrm{km^2}$.

Each REW in the domain has one stream reach with a '`from_node`' and '`to_node`' attribute that identify the upstream and downstream node of the reach. This information is used to build the network topology and a node adjacency matrix that is used in the the water routing algorithm described in Appendix A. Water diversions occur at 56 selected river nodes, one for each economic unit (county) included in the simulation.

we ran the model with daily gridded precipitation, maximum and minimum air temperatures at a 4km resolution, automatically retrieved as NetCDF files from the gridMET dataset (Abatzoglou, 2013). Temperatures are used internally by the model to calculate reference crop evapotranspiration using the Hargreaves method (George H. Hargreaves and Zohrab A. Samani, 1985).

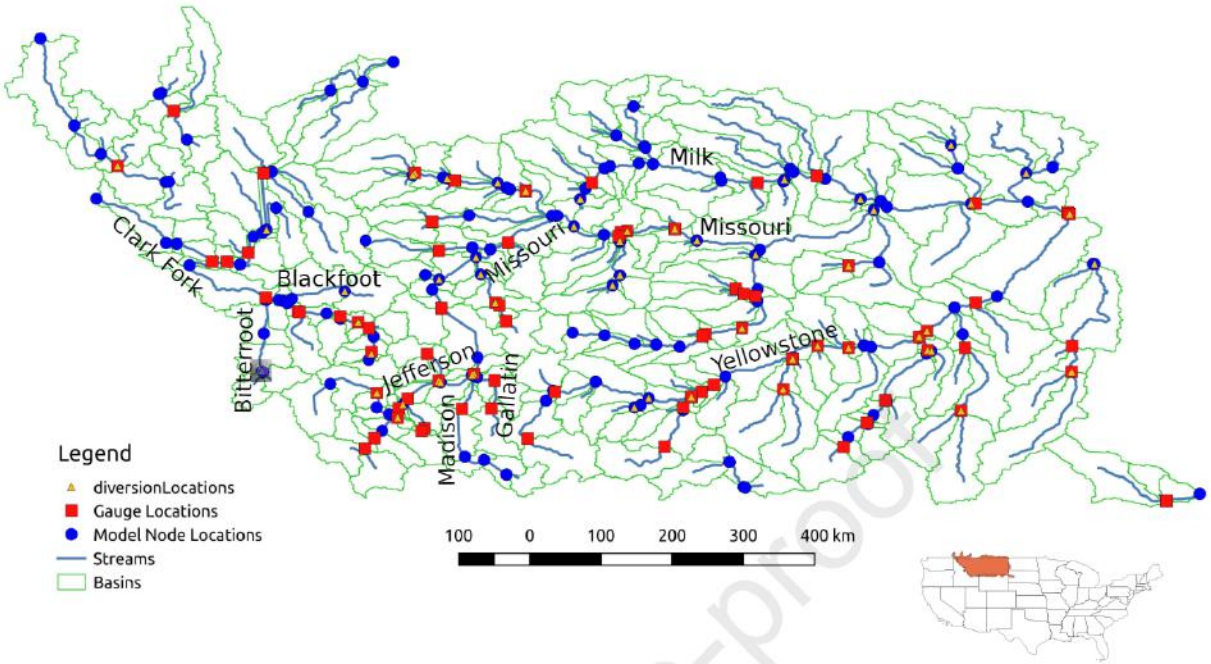

Figure 3: Location of the study region and representation of the hydrologic system and streamflow network

4.1.1. Calibration of hydrologic component

The hydrologic model parameters were calibrated manually against streamflow observations at gauged river nodes and against snow water equivalent observations from the SNOTEL network. All parameters of the HBV rainfall-runoff model and Muskingum-Cunge routing model were adjusted and shared between REWs grouped according to their physiographical (mean elevation, mean slope, area, shape factor) and land use characteristics (fraction of the REW under forest cover and under agriculture) using a standard K-means classification method. In total, we calibrated seven groups of parameters corresponding to seven groups of REWs.

4.2. Implementation of economic component

Although remote sensing can retrieve information about land and water allocation at field scales, the specification of the economic component of our model is designed to simulate the aggregated economic behavior of producers in a region, not the behavior of individual farmers. The economic units considered in this implementation are aggregated at the county level. Thus, we represent the agricultural system in Montana using 56 economic units (counties), each of them retrieving water from the stream network at one designated diversion node. Although the economic activity is represented in aggregated form, intra-county agroeconomic heterogeneity is, to some extent, implicitly captured in the distribution of model predictions for each county.

Table 1: Observations necessary to calibrate the economic component

Observation	Units	Source	Resolution
Land allocation	ha	Remote sensing (National atlas of the United States, 2014)	30 m, 8 day
Water allocation	mm*ha	Remote Sensing (He et al., 2019)	30 m, 8 day
Crop price	$/ton	USDA	State-level, Annual
Cost of land	$/ha		State-level, Annual
Cost of water	$/(mm*ha)		State-level, Annual
Crop production	ton	Remote Sensing (He et al., 2018)	30 m, 8 day
Production elasticity to water	-	Derived, Eq (20)	State-level, Annual
Production elasticity to price	-	Derived, Eq (21)	State-level, Annual

4.2.1. Recursive calibration of the economic component

Information necessary to update the model parameters include land allocated to each crop, total water used by each crop and total crop production. This information is available every year from remote sensing products at 30 m spatial resolution and then aggregated at county scales. In addition, information on crop prices, approximated variable unit costs of cultivating land and cost of applying water are also required (Table 1).

Crop price information and an approximation of production costs were obtained from annual surveys published by the US Department of Agriculture National Agricultural Statistics Service (USDA NASS) at the state scale (QuickStats, `http://quickstats.nass.usda.gov`). Crop coefficients to determine crop development stage were obtained from tables published by the AgriMet network for crops grown in the US Pacific Northwest (`https://www.usbr.gov/pn/agrimet/cropcurves/crop_curves.html`).

Annual variations in crop mix and area are obtained from the USDA Cropland Data Layer, CDL (USDA NASS, 2015), published by the USDA NASS. The CDL provides a satellite-based, remotely-sensed, annual crop-specific land cover classification that resolves the type and location of the major summer crops in the conterminous US. The CDL is available since 2003 for the conterminous US at 30 m spatial resolution. Since the unit of analysis of the economic component is the county, we calculated total allocated land in each county for the main crops grown in Montana (alfalfa, barley durum wheat, spring wheat, winter wheat, maize and peas) from 2009 to 2018. Uncertainty in land allocation retrievals were estimated by scaling the average pixel level classification uncertainty (standard deviation) of each crop by the number of pixels allocated to the crop in the county. Figure 4a shows an example of the CDL and the annual variations in allocated area for alfalfa, barley, spring wheat, and winter wheat in two counties.

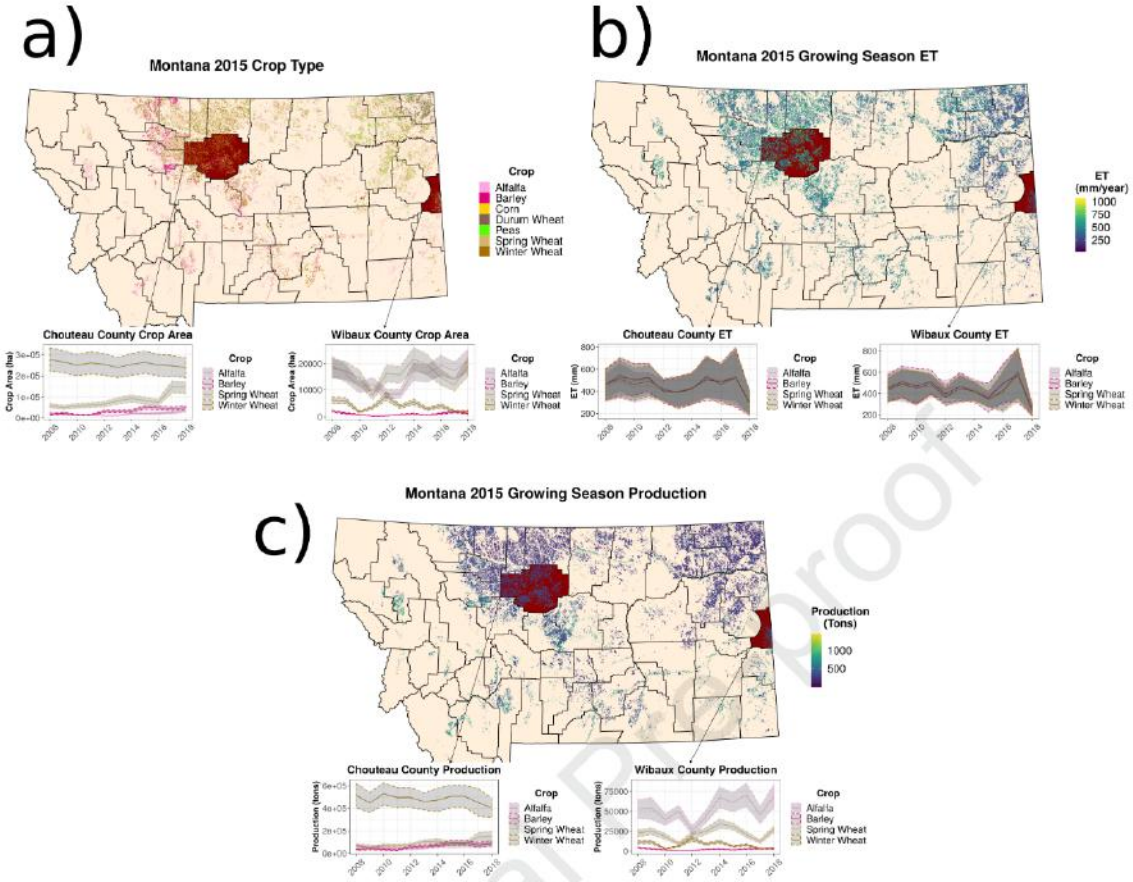

Figure 4: Example of remote sensing retrievals of agricultural activity over the state of Montana. The maps in the figure show pixel-level retrievals in 2009 of a) crop type, location and extent; b) seasonal crop evapotranspiration; and c) crop yield. The time series (insets) show county-aggregated variations of a) total allocated land; b) total county-level crop water use; and c) county-level total production for four example crops (alfalfa, barley, spring wheat and winter wheat) and two example counties (Choteau and Wibaux).

Observations of crop production and yield (defined as the ratio of production to area planted) were obtained using a satellite-driven, light-use efficiency model to estimate gross primary production (GPP) over croplands at 30 m resolution and 8-day time step. The high spatial and temporal resolution necessary to delineate cropland vegetation growth was achieved by using a NDVI dataset that blended Landsat 5/7 reflectance and Terra MODIS reflectance. Crop yields each year were obtained by accumulating GPP over the growing season and applying a crop-specific harvest index to convert primary production to yields. He et al. (2018) gives a full description and validation of this remote sensing product. We calculated county-scale annual crop production by multiplying crop yield times the area allocated to the crop in each county. Uncertainty in the county-scale production estimates was obtained by scaling the spatial standard deviation of yields by the area planted. Figure 4c shows an example of the 30 m remotely-sensed retrieved yield map and the annual variation of alfalfa, barley, spring wheat, and winter wheat production from 2009 to 2018 in two counties.

Crop water use was estimated by adapting an operational global ET product (NASA MOD16A2 Mu et al., 2011). To better represent cropland ET, our adaptation of the MOD16A2 product uses finer scale meteorological inputs from the GridMet product (Abatzoglou (2013)), and the same refined 30 m resolution NDVI dataset used in the estimation of production. The model parameters were also recalibrated for broadleaf crops, and for cereal crops. A complete description of the adaptation of MOD16A2 ET product for agricultural applications of the conterminous US is given by He et al. (2019). Annual variations in county-scale, crop-specific water use volumes were calculated by accumulating pixel-scale ET over the growing season and at the county scale for each crop. Uncertainty in the county-scale water use estimates was obtained by scaling the spatial standard deviation of crop ET by the area planted. Figure 4b shows an example of the 30 m remotely-sensed retrieved crop ET map and the annual variation of total water volumes used by alfalfa, barley, spring wheat, and winter wheat production from 2009 to 2018 in two counties. Note that crop water use includes both evapotranspiration from precipitation and from supplemental irrigation.

4.3. Analysis methods

For this analysis we set the ensemble size $M = 300$. To stabilize model parameters and start with correct (optimal) values at the beginning of the analysis period, we first spun up the data assimilation process by repeatedly assimilating observations from 2008 (first year in our data record) until the posterior distribution of the model parameters converged. We tuned the filter by manually adjusting the variance smoothing parameter h and the background parameter ensemble variance ($\mathbb{V}^*_{\cdot,k}$) until the parameter ensemble resulted in land allocation prediction distributions that approximated the assumed distribution of land allocation observations in 2008. We found good results assuming $\mathbb{V}^*_{\beta_{land},k}$, $\mathbb{V}^*_{\beta_{water},k}$, $\mathbb{V}^*_{\delta,k}$, and $\mathbb{V}^*_{\mu,k}$ were 0.01 of the square of their respective ensemble means. We found $\mathbb{V}^*_{\lambda_{water},k}$, $\mathbb{V}^*_{\lambda_{land},k}$ and $\mathbb{V}^*_{\overline{\lambda}_{fsl},k}$ to be very sensitive to errors and required a smaller variance of about 0.0001 of the square of their respective ensemble means. We also prescribed $h = 0.97$ and $a = 0.94$ (low level of parameter smoothing).

After the spin up was complete (e.g. parameters converged to their optimal or near-optimal values from their arbitrary initial values), we used the resulting model parameters to verify that they correctly reproduce the observed land and water allocations used to calibrate them. After this verification, we started the data assimilation process by sequentially ingesting observations from 2008 to 2016. Observations from 2017 and 2018 were available but not ingested and used to verify the the ability of the model to predict out of sample years. We focused model verification and analysis mostly on predictions of land and water allocation, since it is one of the most novel aspect of the modeling system. However, we also demonstrated the value added by the hydrologic component by identifying the net impact of agricultural water diversions in 2017. In the discussion section we provide a qualitative evaluation of the spatial impacts of agricultural water use.

Table 2: Mean relative bias (Rel. Bias [a]) and relative root mean square error (Rel. RMSE[b]) statistics for the simulation land allocated during the 2008 benchmark conditions.

	2008			
	Land Use		Water Use	
	Rel. Bias	*Rel. RMSE*	*Rel. Bias*	*Rel. RMSE*
Alfalfa Irrigated	-0.072	0.090	-0.174	0.218
Alfalfa Nonirrigated	-0.044	0.087	-	-
Barley Irrigated	-0.050	0.099	-0.087	0.255
Barley Nonirrigated	-0.030	0.068	-	-
Spring Wheat Irrigated	-0.029	0.090	0.080	0.246
Spring Wheat Nonirrigated	-0.030	0.110	-	-
Winter Wheat	-0.028	0.110	-	-

[a] $Rel.Bias = \frac{sim_i - obs_i}{obs_i}$

[b] $Rel.RMSE = \frac{\sqrt{\frac{1}{n}\sum_i^n (sim_i - obs_i)^2}}{\frac{1}{n}\sum_i^n obs_i}$

5. Results

5.1. Calibration and verification: parameter spin-up

The results of the parameter spin-up showed that for most counties the parameters could be accurately inferred from the assimilated observations. An example for Beaverhead county (a county with a large extent of land allocated to agriculture and also first county alphabetically) is shown in Figure 5. Results for all counties are presented in Appendix A available online. The ensemble was initiated before the spin-up with an arbitrary mean and a large spread (initial coefficient of variation of the ensemble was prescribed at 100%) and the ensembles typically converged to a steady state distribution with within five to eight assimilation cycles. Figure 6 show the dynamics of the ensemble of innovations (residual between Eq. (16) and Eq. (17)) for the parameter evolution of Beaverhead county shown in Figure 5. The figure shows that the innovation quickly approaches zero, which indicates that the parameter ensembles converge to a solution that satisfied the optimality conditions of the positive mathematical program (Eq. (B.2)). The algorithm works because components (1) and (2) in Eq. (16) represent the marginal revenues with respect to land and water allocation, and components (1) and (2) of Eq. (17) represent the respective marginal costs. When the ensemble of differences between LHS_i and RHS_i is centered about zero the methodology is effectively solving the first order conditions of the net revenue maximization problem, which is the core of the calibration algorithm. Online Appendix B shows the evolution of the innovation ensembles associated with the parameter spin-ups in all counties in the state of Montana. An inspection of this appendix shows that all innovations reliably have zero mean and a steady variance, which are diagnostics of the correct performance and tuning of the

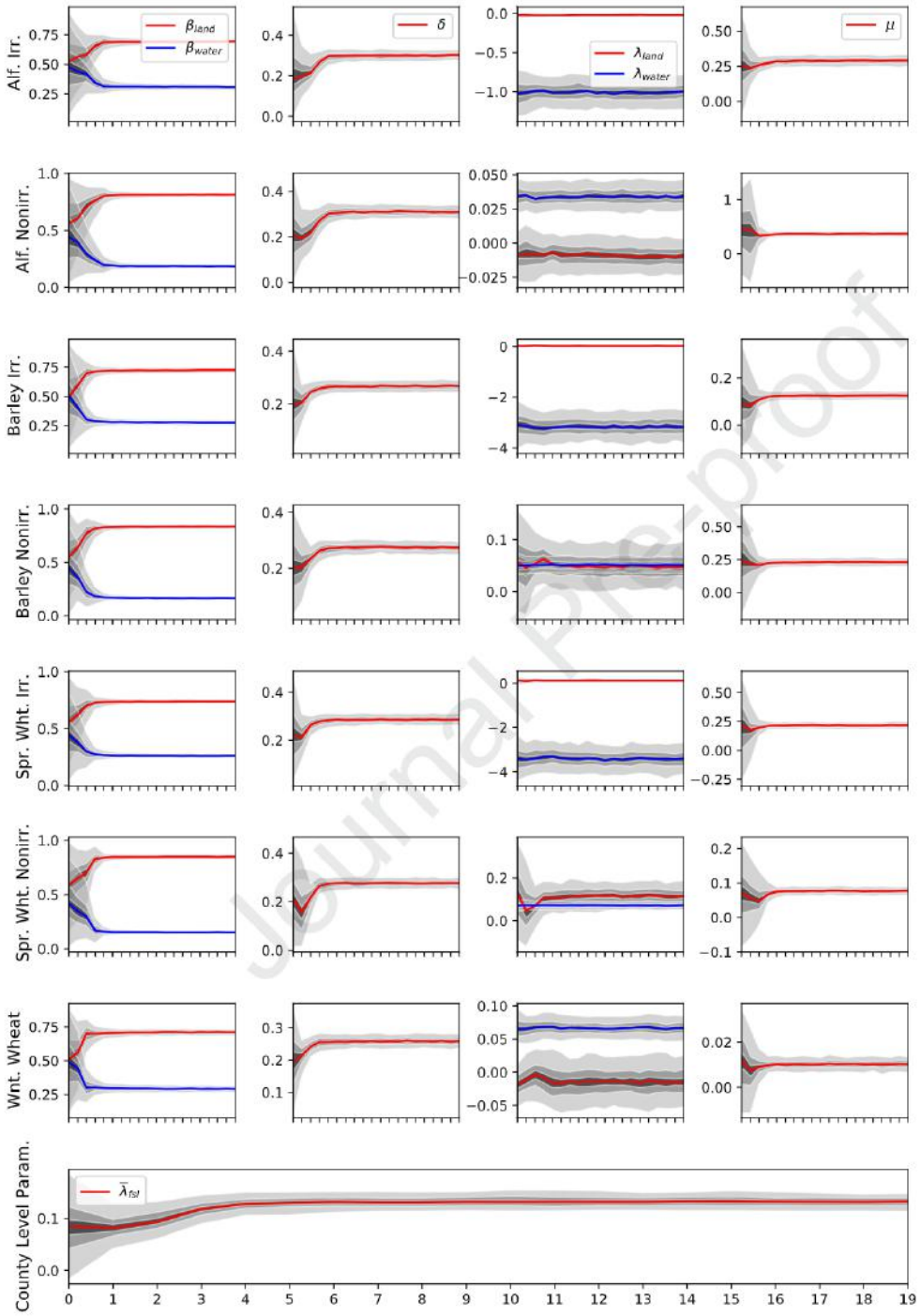

Figure 5: Evolution of the parameter ensemble during parameter spin-up in Beaverhead county. Shaded areas are the 95 and 68 percentile confidence intervals of the ensemble. Ensembles for all counties is presented in online Appendix A

The ensemble of parameters obtained at the end of the spin-up cycle was used to predict the land and water allocation for the 2008 baseline. The model was able predict mean land and water allocations in each county with satisfactory accuracy, as summarized in Table 2. The correlation coefficient between county-wise simulated and observed land allocation is higher than 0.98 and the relative bias of the estimation is typically less than 0.06 (6%).

A comparison between the predicted probability distributions of land and water allocation and observed allocations provides a direct evaluation of the model predictive skills for individual counties and also illustrates how parameter uncertainty translates into uncertainty in the predictions of resource allocation. Figure 7 shows the simulated probability distribution of land allocated to the crops grown in Beaverhead county along with the observations. The assumed uncertainty in the observed land allocation was used to tune the background variance of the parameters and provide additional confidence that the filter is correctly tuned. Online appendix C shows the simulated land allocation for all crops and counties. In general, for all counties and crops, the predictive distributions are well centered around the observation and have a variance that approximate the assumed observational error.

Comparison between observed and modeled water allocation for irrigation is less straightforward because water allocation per crop and county is not directly observed. Remote sensing ET observations only provide total crop water use, which integrates water from natural precipitation and from supplemental irrigation. However, the simulation scenarios require that the the expected amount of water from natural sources used by crops (natural ET) is specified. Subtracting this specified natural ET amount from the total observed crop water use gives us an estimate of the amount of crop water use supplemented by irrigation. This estimate served as the observation of supplemental irrigation used to evaluate the model simulation of water allocation. Figure 8 shows the case of Beaverhead county. Figures for water allocation in all counties in the state are provided in online appendix D. Similar to the simulation of land use, the simulation of water allocation per crop and county is also centered around the observations, bracketing them in most cases within the high probability region of predictions.

5.2. Dynamics of the parameter ensemble

Using the parameter distributions obtained at the end of the spin-up period as a starting point, we assimilated remote sensing observations from 2009 through 2016. Figure 9 shows the dynamics of the parameter ensembles for Beaverhead county over the the eight years of data assimilation. Note that the y axis has been re-scaled with respect to that of Figure 5 to better represent the ensemble spread. Figures for all counties are available in online appendix E. In general, parameters β_{land} and β_{water} showed very high stability and very little dispersion over time, with very small drifts in their mean value. To a lesser degree, parameter δ also presented relatively high stability but higher ensemble dispersion. On the other hand, λ_{land}, λ_{water}, and the μ parameters showed large ensemble dispersion and high sensitivity to variations in the input observations. The evolution of the parameters sometimes exhibited drifts over the data assimilation period (e.g. parameter

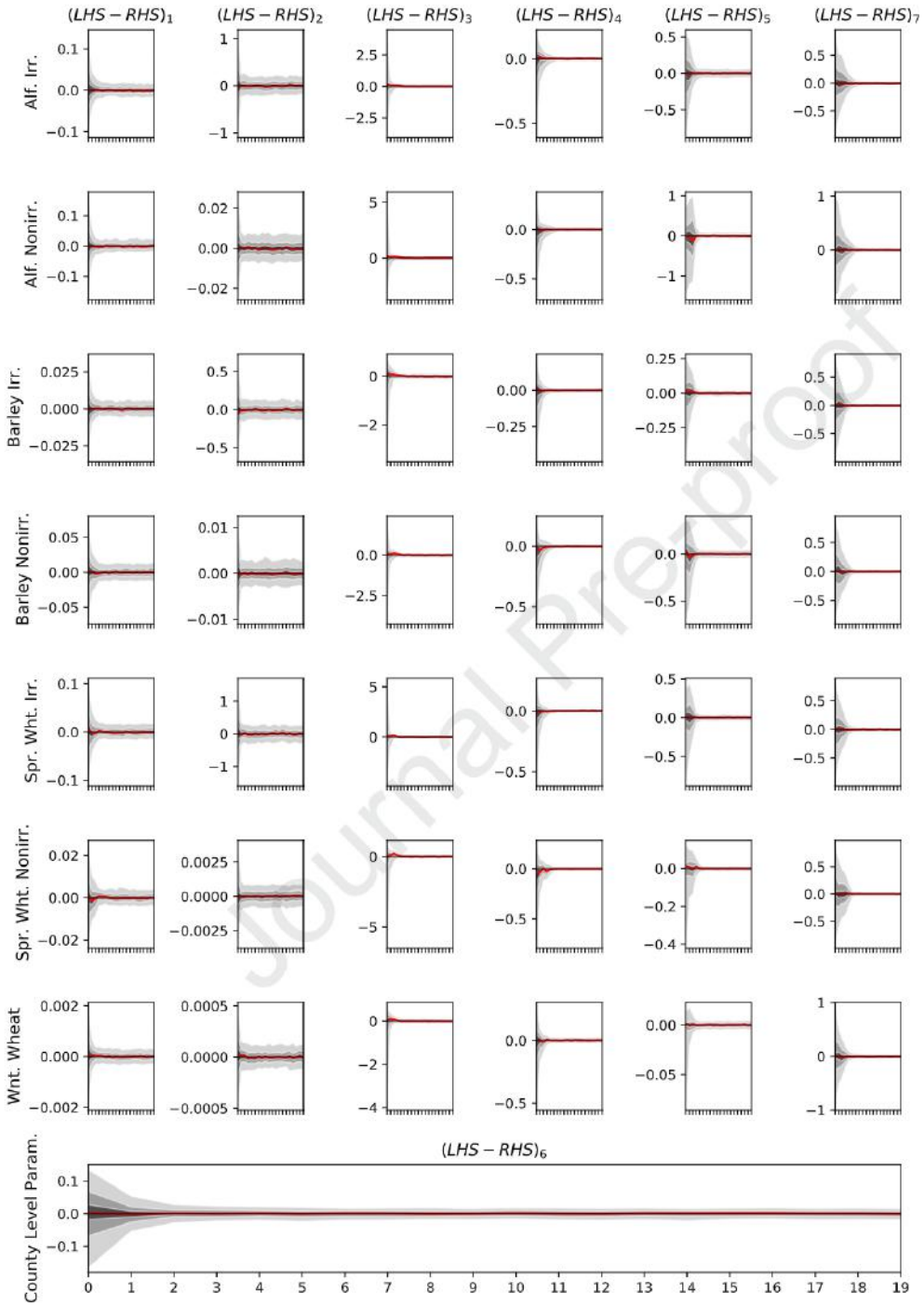

Figure 6: Evolution of the filter innovation during parameter spinup corresponding to the ensembles in Figure 5. Subscript of column titles refer to a innovation component as numbered in Eqs. (16) and (17). Shaded areas are the 95 and 68 percentile confidence intervals of the ensemble. Ensemble for all counties is presented in online Appendix B

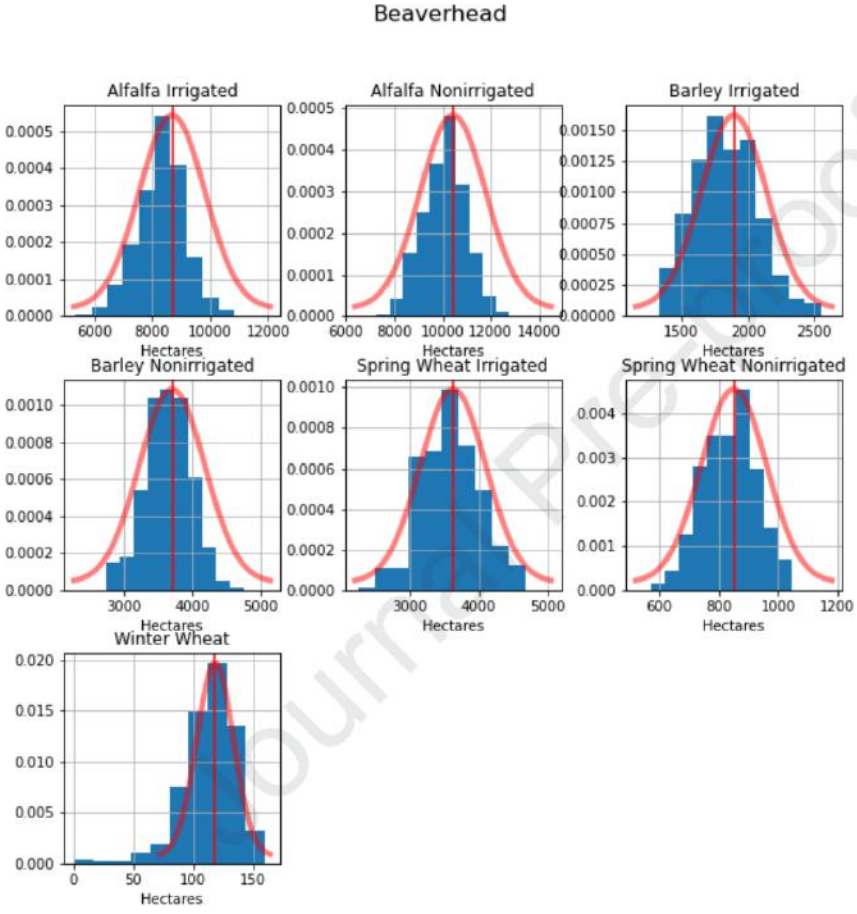

Figure 7: Simulated probability distributions (blue bars) and observed probability distribution (red line) for land allocation in 2009 for seven crops grown in Beaverhead county, MT. The assumed observation error shown in this figure was used to tune the filter. Simulations for all counties is presented in online Appendix C.

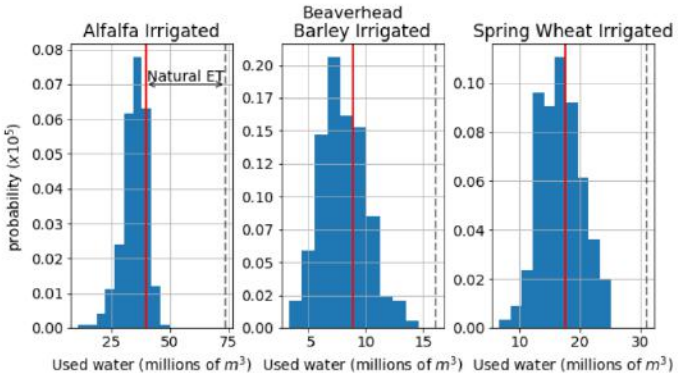

Figure 8: Simulated probability distribution of water allocation for three irrigated crops grown in Beaverhead county, MT (blue bars). Dashed grey vertical line indicates the observed total evapotranspiration consumed by the crop (evaporation from natural supplies and from supplemental irrigation). Benchmark supplemental irrigation (red vertical line), was estimated by subtracting water used by crops from natural supplies (natural ET) as prescribed in the modeled scenario from the observed total crop evapotranspiration. Simulations for all counties is presented in online Appendix D.

winter wheat and $\overline{\lambda}_{fsl}$ in year 2010), or fluctuations about a long term mean without a clear trend (e.g. parameter μ for winter wheat in Figure 9)).

The dynamics of the innovation associated with the parameter ensembles in Fig.9 were in general tightly centered around zero for most components, reflecting the performance of the filter(Figure 10). The filter maintained most of the parameters at optimal values for operational use throughout the assimilation period. Components (1) and (2) of the innovation showed the highest variance but not significant biases. The most significant departures of the ensemble from zero where for winter wheat, but these were only transient. Although Figure 10 represents the case for one county (Beaverhead county), component (2) of the innovation was often the one that exhibited the largest amount of bias and variance over all counties (See Appendix F). This component of the innovation is controlled by parameter λ_{water_i}, which is one of the most sensitive parameters of the model and is key to correctly reproduce the correct allocation of water.

Figure 11 and Figure 12 show the state-wide interannual variability of modeled land allocation and mean annual crop water use generated by running the model using the parameter ensemble obtained at the end of the assimilation period. The figure shows time series obtained by averaging results over all counties during the 2008-2016 calibration period. Relative prediction biases and relative root mean square error statistics are given in Table 3. The model captures the magnitude of the observed land allocation to each crop type and the share of land that is irrigated and non-irrigated, although some biases are apparent. Also, especially in the case of alfalfa, the model exhibits larger interannual variability than the observations (Figure 11a). A small high-bias and higher variability in modeled mean water use is also apparent (Figure 12 and Table 3). The whiskers and shaded area in these figures are the interquartile range of the county-level observations and predictions, respectively, and give us information of their spatial (inter-county) variability. In general, the inter-quartile range of observations and predictions is similar in the case of crop allocation (Figure 11),

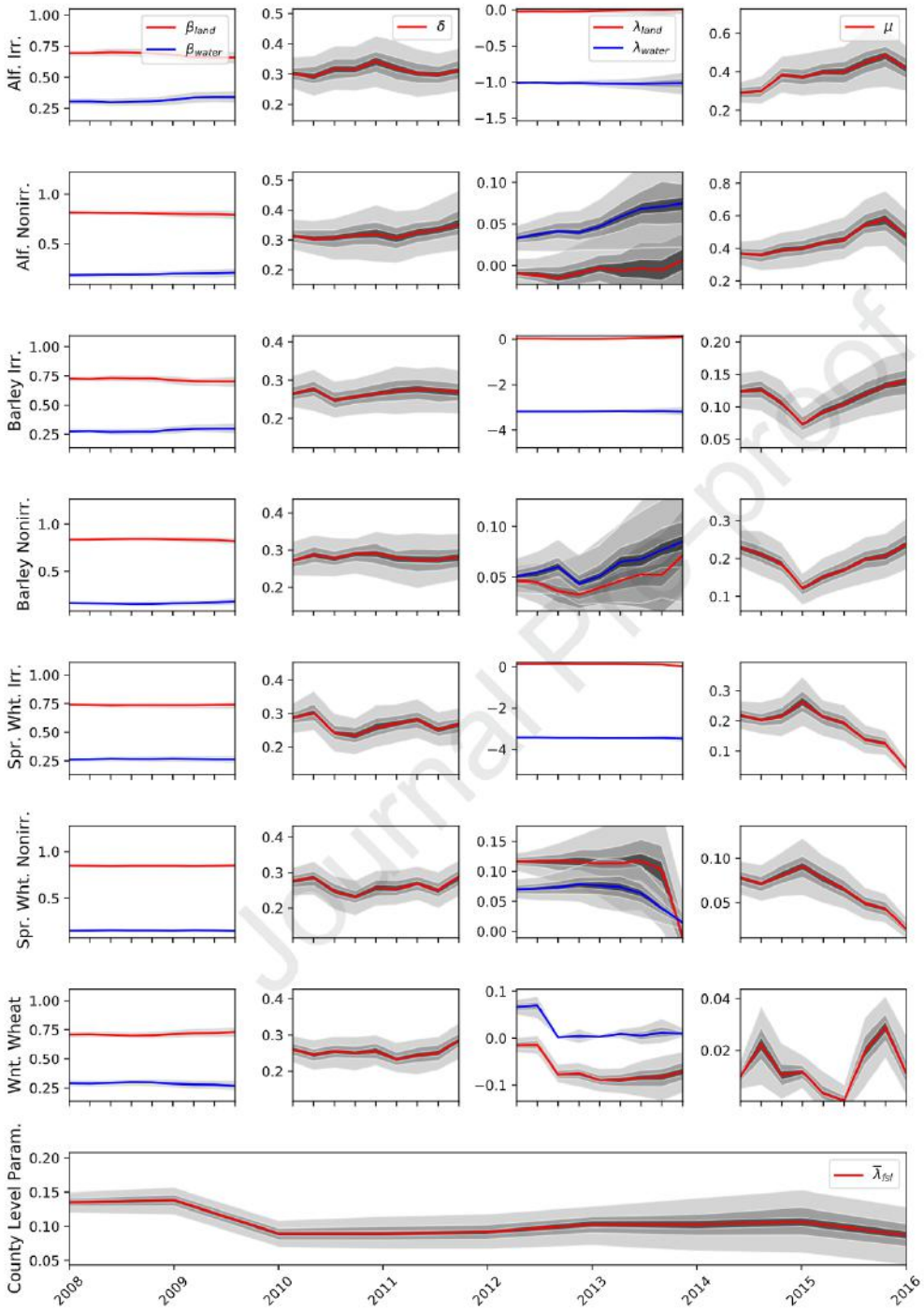

Figure 9: Dynamics of the parameter ensembles over 8 years (2008-2016) of data assimilation in Beaverhead county. Parameters start from the distribution achieved at the end of the spin-up period in 2008. Shaded areas are the 95 and 68 percentile confidence intervals of the ensemble. Figures for all other counties are presented in Online Appendix E.

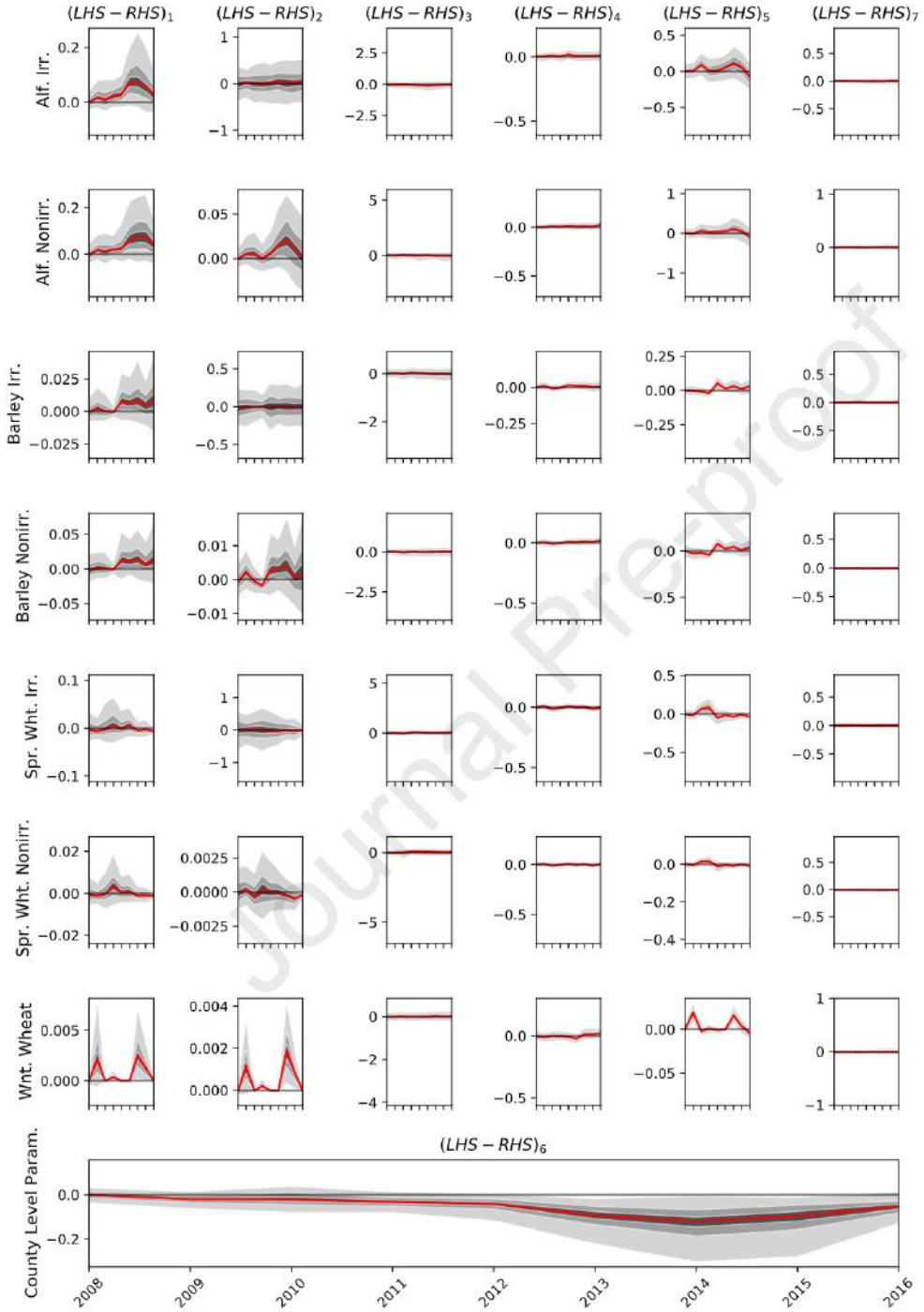

Figure 10: Dynamic of the innovation over 8 years (2008-2015) of assimilation corresponding to the parameter ensembles shown in Figure 5. Subscript of column titles refer to a innovation component as numbered in Eqs. (16) and (17). Shaded areas are the 95 and 68 percentile confidence intervals of the ensemble. Ensembles for all counties are presented in online Appendix F

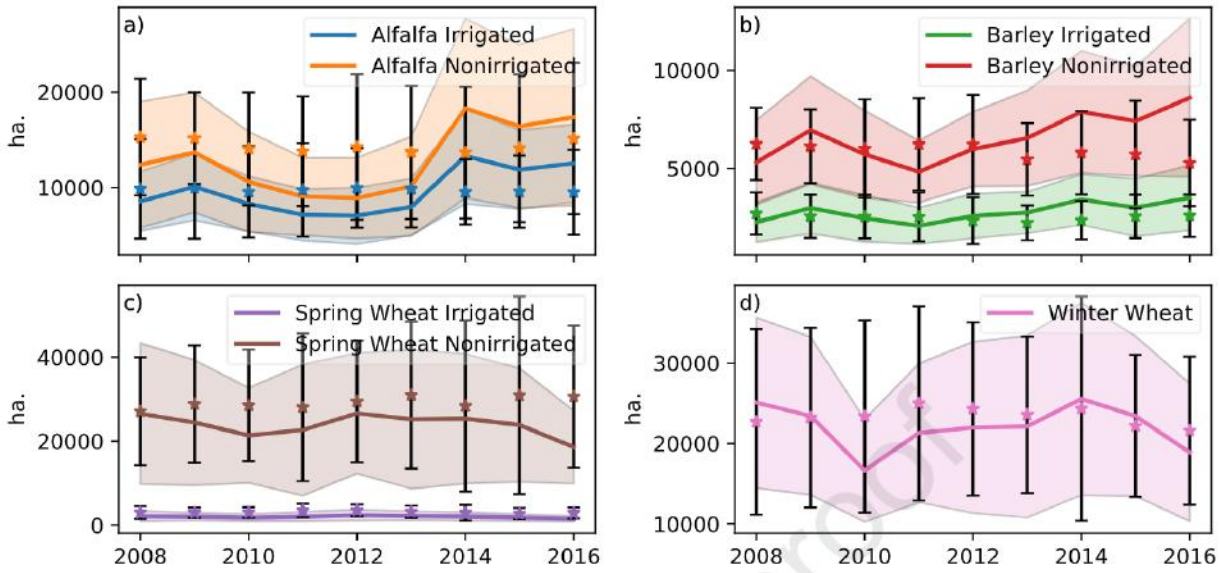

Figure 11: Modeled (lines) and observed (markers) average land allocation over the 2008-2016 calibration period. Shaded areas and error bars represent the inter-quartile range of the distribution of county means for the modeled and observed land allocations, respectively. The interquartile range provides a sense of the spatial variation of land allocation between counties.

water use (Figure 12) underestimate the observed spatial variability. Despite the biases, the simulations clearly discriminate the crops that are prioritized by farmers, and to simulate a spatial distribution that is on par with the predictions. This is further shown in the next section, which focuses on the simulation of two out-of-sample years.

5.3. Simulation of years 2017 and 2018

Table 4 shows the relative bias and root mean square relative error (RMSRE) of the mean predicted vs observed crop acreage and water allocation over all counties in Montana for years 2017 and 2018. For these simulations, the model was run with the parameter distribution obtained at the end of the 2008-2016 assimilation period. Year 2017 is associated with the abnormal conditions generated by the severe flash drought that affected the US Northern Plains in the summer of 2017 (He et al., 2019; Kimball et al., 2019). Despite of this, the results for the two simulated years are qualitatively very similar and therefore we only present and discuss the predictions for year 2017. The discussion of the results from 2017 also apply to the simulations of year 2018.

The model satisfactorily reproduced the county-scale distribution of cropping patterns (Figure 13). Alfalfa is grown in all counties and the model predictions capture well the spatial distribution of land allocation for this crop (Figure 13 rows 1 and 2). Note that the area planted with non-irrigated alfalfa tends to be larger in the eastern third of the state because that region is characterized by large properties and extensive ranching. This distribution is well captured in the model predictions. On the other hand, irrigated alfalfa is more

Table 3: Mean relative bias (Rel. Bias) and relative root mean square error (Rel. RMSE) statistic of the prediction of county average land per crop and water allocation over the 2008-2016 calibration period.

	Rel. Bias	*Rel. RMSE*
Alfalfa Irrigated	0.063	0.273
Alfalfa Nonirrigated	-0.024	0.262
Barley Irrigated	0.123	0.222
Barley Nonirrigated	0.140	0.275
Spring Wheat Irrigated	-0.370	0.377
Spring Wheat Nonirrigated	-0.169	0.205
Winter Wheat	-0.099	0.173
Water use (Fig. 12)	0.370	0.411

$$Rel.Bias = \frac{sim_i - obs_i}{obs_i}$$

$$Rel.RMSE = \frac{\sqrt{\frac{1}{n}\sum_i^n (sim_i - obs_i)^2}}{\frac{1}{n}\sum_i^n obs_i}$$

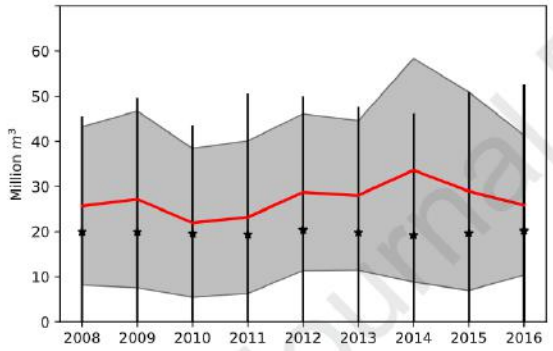

Figure 12: Modeled (lines) and observed (markers) average annual effective crop water use from supplemental irrigation over the 2008-2016 calibration period. Effective crop water use is defined as the fraction of applied water that is used by crops. Shaded areas and error bars represent the inter-quartile range of the distribution of county means for modeled and observed irrigation, respectively. The interquartile range provides a sense of the spatial variation of water allocation between counties.

Table 4: Mean relative bias (Rel. Bias [b]) and relative root mean square error (Rel. RMSE [b]) statistic of the prediction of land and water allocation for out-of-sample years 2017 and 2018.

	2017				2018			
	Land use		Water use		Land use		Water use	
	Rel. Bias	*Rel. RMSE*	*Rel. Bias*	*Rel. RMSE*	*Rel. Bias*	*Rel. RMSE*	*Rel. Bias*	*Rel. RMSE*
Alfalfa Irrigated	-0.003	0.151	-0.182	0.425	-0.067	0.182	-0.21	0.547
Alfalfa Nonirrigated	0.155	0.277	-	-	-0.045	0.133	-	-
Barley Irrigated	0.319	0.305	2.561	1.472	-0.193	0.379	4.91	1.460
Barley Nonirrigated	0.301	0.476	-	-	-0.155	0.226	-	-
Spring Wheat Irrigated	1.321	0.540	3.026	1.26	2.531	0.508	2.19	1.54
Spring Wheat Nonirrigated	-0.005	0.285	-	-	-0.037	0.165	-	-
Winter Wheat	-0.241	0.488	-	-	-0.167	0.089	-	-

[a] $Rel.Bias = \frac{sim_i - obs_i}{obs_i}$

and in the upstream end of the Gallatin, Yellowstone and Missouri rivers. This is also correctly captured by the model. Also remarkable is the ability of the model to identify the regions in the state that specialize in small grain production. The model correctly identifies the counties in the west and north west central region of Montana that allocate the most land to irrigated and non-irrigated barley (Figure 13 rows 3 and 4). It also identifies very well the swath of counties in the north and north east portions of the state that allocate the most land to grow spring wheat and winter wheat (Figure 13 rows 5 and 6). The spatial distribution of relative errors show some complex spatial patterns, but in general relative errors in simulated area allocated to a crop are largest in counties where observations of area planted with a given crop are small because relative errors are normalized by these observations. This causes the summary statistics presented in Table 4 to be skewed by very large errors in a small number of counties. This is particularly evident in the statistics of land allocated to irrigated barley and irrigated spring wheat, where simulated land allocation tends to underestimate observations (negative relative errors represented by blue colors in Figure 13), but Table 4 reports a large positive relative bias.

The extent of land allocated to irrigated crops is, of course, an indication of the agricultural water demands. In general, agricultural water use is higher in counties that are closer to the river headwaters. Counties in the headwaters of the Missouri river and upstream tributaries (Jefferson, Madison and Gallatin Rivers, see Figure 3), in the southwestern quadrant of the state, as well as counties in the upper course of the Yellowstone river in south central Montana, have some of the highest agricultural water consumption in the state, putting a significant amount of strain on the water supplies. This agricultural water consumption pattern is clearly represented in the simulated total agricultural applications per county (Figure 14). The model underestimated the total agricultural water use in all counties (negative relative errors), however the relative underestimations are in general modest. Large relative errors in the predictions often occur in counties with relatively low observed supplemental irrigation.

Counties with high agricultural water use are expected to have the largest impacts on the hydrologic system. A strength of hydro-economic model is that it tracks the hydrologic impacts of agricultural activity. The spatial and temporal net effects of agricultural diversions on streamflows are shown in Figure 15. Insets in Figure 15a show simulated streamflows with and without the effects of water diversions for year 2017 in four nodes of the river network and the simulated water diversion rates from these nodes during the growing season. The standard profile of water diversion rates in all nodes followed the water demands associated with the progression of crops during the growing season. Water withdrawals start on the prescribed planting date of each crop, which for most crops is around May 15, increase as crops grow to full coverage, and finally taper down as crops mature before the prescribed harvesting date in late August. The impacts of water withdrawals on streamflows starts during the spring freshet, when streamflows are high, but it is typically maximal in late June or early August during low summer flows. When water diversions decline at the end of the summer, the model simulates the recovery of streamflows.

The spatially distributed nature of the hydrologic model naturally simulates the downstream impacts of

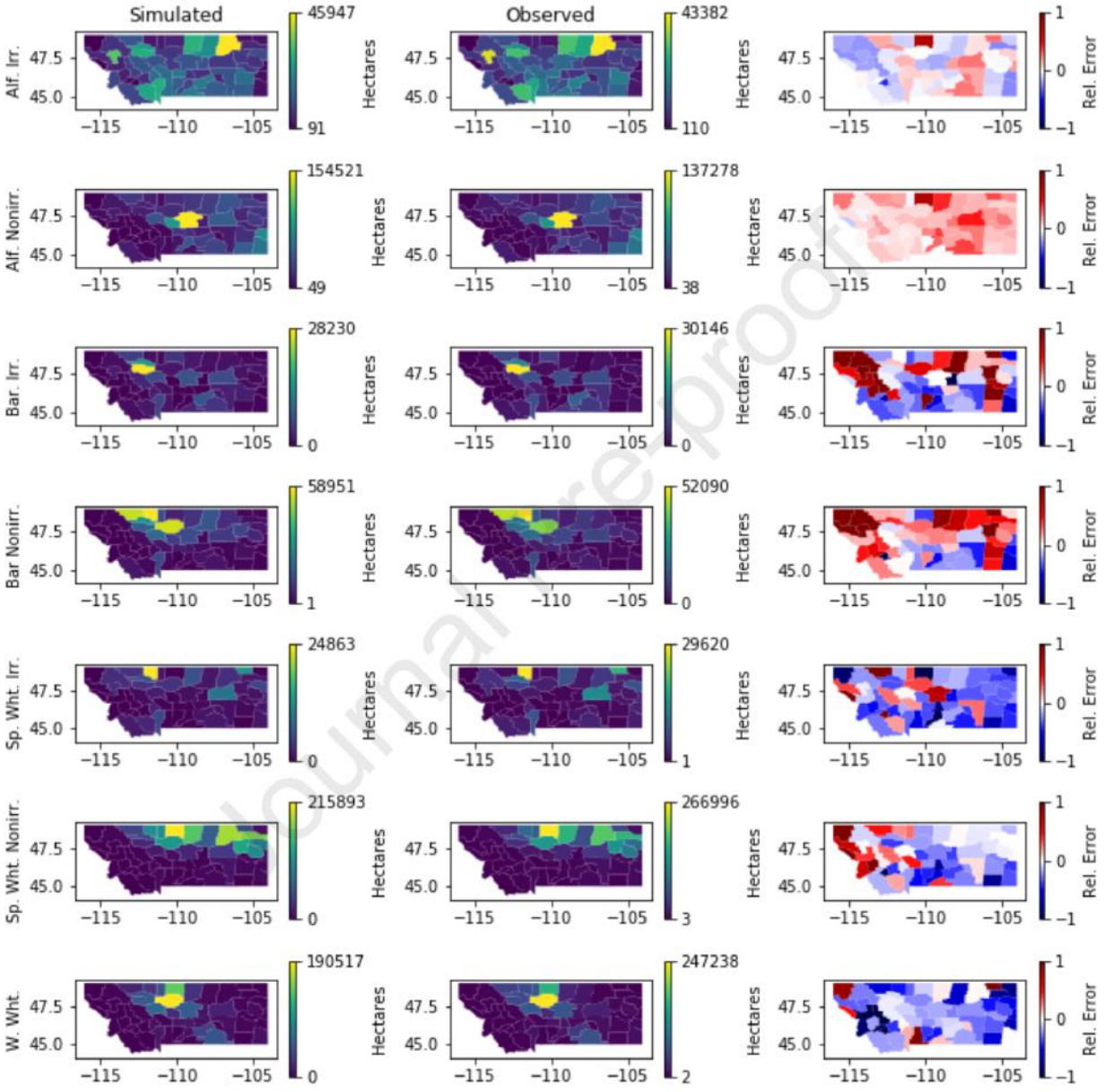

Figure 13: Comparison between model simulated (left column) and observed (center column) land allocated in 2017 to the major crops grown in Montana. Right panel shows the relative prediction error defined as $\frac{simulated-observed}{observed}$. Counties with small amounts of observed land allocated to a given crop can produce disproportionately large relative errors. For visualization purposes, the error scale has been clipped to values from -1 to 1..

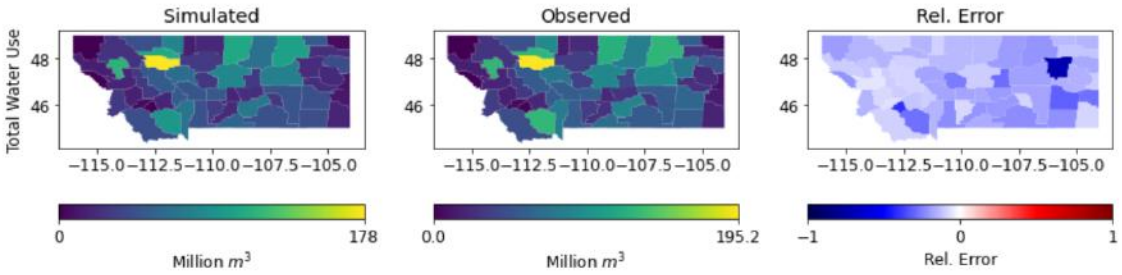

Figure 14: Comparison between simulated (left panel) and observed (center panel) total agricultural water applications per county for year 2017. Right panel shows the relative prediction error defined as $\frac{simulated-observed}{observed}$. Counties with small amounts of observed irrigation can produce disproportionately large relative errors. For visualization purposes, the error scale has been clipped to values from -1 to 1.

agricultural activity. For instance, the inset associated with the easternmost node in Figure 15a is not a diversion node, so there are no agricultural water withdrawals from this location, however water diverted upstream still reduces the natural flows in late spring and summer. To appreciate better the spatial extent of streamflow drawdowns, we produced a visualization of the total net impact of agriculture on the hydrologic network in 2017 (Figure 15b). The net impact (Δ Streamflow) was produced by calculating the total annual water volume difference between natural flows and flows under agricultural withdrawals. Unsurprisingly, the most impacted river reaches are those that supply water to counties with high agricultural water applications, such as those in the headwaters of the Missouri river (c.f. Figure 14), however the impact of water diversion often extends far downstream, affecting counties where agricultural water demands are low.

6. Discussion

The implementation of the economic component of our hydro-economic model uses the stochastic and recursive data assimilation framework based on the ensemble Kalman filter proposed by Maneta and Howitt Maneta and Howitt (2014), however the new implementation adopts the form of the optimality conditions for calibration proposed by Mérel et al. (2011) and Garnache et al. (2017). The implementation of the positive mathematical programming methods proposed by these authors has two major advantages over the standard implementation used by Maneta and Howitt (2014). One advantage is that it eliminates the need to solve an initial linear constrained optimization problem to identify the unknown Lagrange multipliers associated with land and water constraints (Howitt, 1995). Another important advantage is that it does not require a quadratic or exponential specification of the land cost function used in the standard implementation to provide the response function with the correct curvature (Howitt, 1995; Howitt et al., 2012a).

Our analysis demonstrates that information on land use, crop evapotranspiration and crop production from existing and newer satellite-based remote sensing products contain sufficient information to calibrate the hydro-economic model presented here. It also shows that the recursive data assimilation methodology is

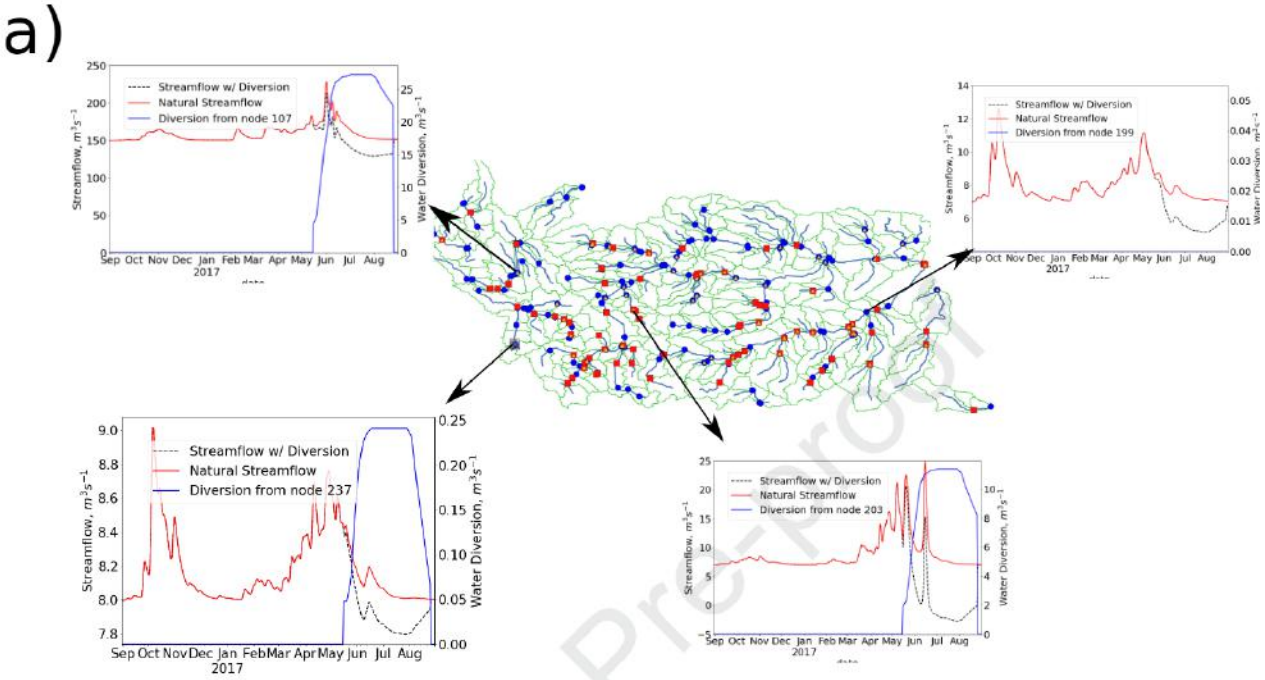

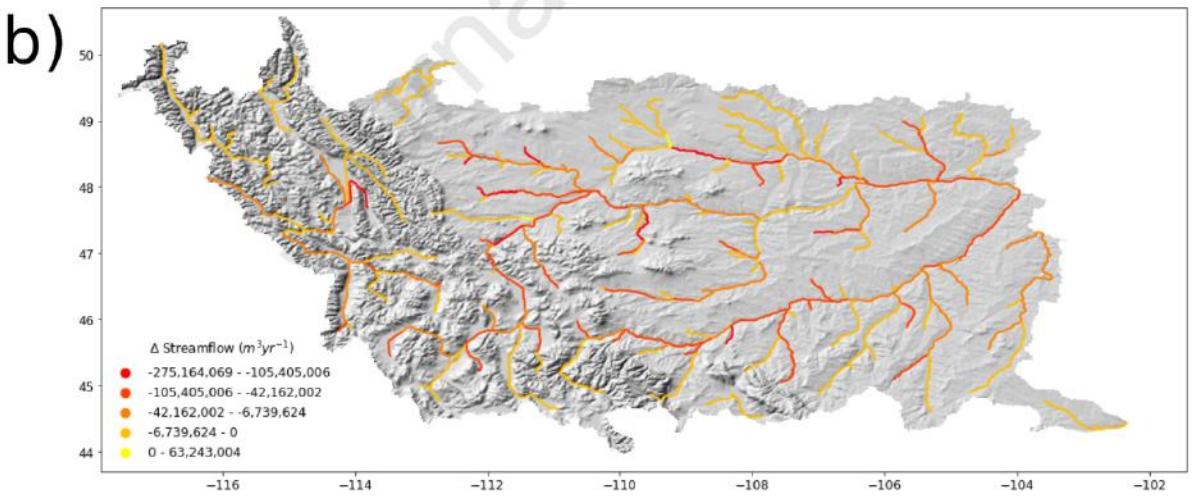

Figure 15: Simulated hydrologic conditions during the 2016-2017 water year. Insets in a) show time series of simulated streamflows assuming no agriculture (red line), simulated streamflows with diversions (black dotted line), and agricultural water diversion (blue line) for four nodes in the river network. Panel b) shows the spatial impacts of agriculture on total annual streamflow volumes. *Delta* Streamflow is the difference in total annual simulated streamflow volumes between the no agriculture reference model and the model with active agricultural diversions.

small number of assimilation cycles. Furthermore, The recursive updating nature of the filtering algorithm is ideal for model applications in non-stationary systems because it adapts the model calibration to the realities of the regional agriculture. Variations in the model parameters over time may be indicative of changes in the economic behavior of farmers triggered by external factors that may not be directly or easily detectable from satellite-based remote sensing information (e.g soil fertility) or due to shifting farmer perception or management practices. For instance, the recursive calibration for Beaverhead county (Figure 9), shows that parameter δ, which represents the production returns to scale, may be slowly increasing over time for nonirrigated alfalfa while remaining relatively stable for other crops. Values less than unity for this parameter indicate that crop production will increase exponentially less than a given increase in land and water allocated to this crop. Decreasing returns to scale reflect agricultural realities like the likelihood that crops expand to land of lessening quality, or the diminishing returns of additional water applications when crops are irrigated near their optimal level. Upward trends of this parameter signal technical or management improvements over our study period that increase productivity returns from land and water inputs. On the other hand, Parameter mu, which is a factor that represents the efficiency of the production system, seemed to decline for irrigated and non-irrigated spring wheat. Declines in this factor indicate loss of county production in these crops that cannot be explained by a reduction in the amount of land and water allocated to these crops. For instance, if may signal loss of soil fertility or declines in other inputs not explicitly included in the model. Note that the sensitivity of the model parameters to new observations is dependent on the value of a in the parameter blending Eq. (12). This a factor was prescribed at a value of 0.94 for this analysis, which provides a low level of smoothing and results in model parameter more responsive to new information. Lower values of a decrease the calibration sensitivity to new observations.

An important characteristic of economic models of agricultural production calibrated using the PMP methodology is that there is no need to know with precision the production costs because the calibration algorithm approximates unknown or unspecified production costs by adjusting the $\lambda_{land,i}$ and $\lambda_{water,i}$. In our implementation of the optimality conditions, negative λ_i values for land or water indicate that there are unobserved benefits associated with these inputs, which is to say that the observed production costs, c_{land_i} and $c_{water,i}$, are overestimated. Conversely, a positive $\lambda_{i,l}$ value means that the observed production costs are under-estimated. In general, and in the case of Beaverhead county (Figure 9), irrigated crops typically have a negative value for $\lambda_{water,i}$, while positive values are more common in non-irrigated crops.

The capacity to estimate the value of $\lambda_{water,i}$ is an important characteristic of the calibration method, however this parameter is often the most unstable during the data assimilation process and probably one of the largest sources of uncertainty in model predictions, as diagnosed by biases in component (2) of the innovation (Figure 10). Errors in the identification of this parameter may be the largest source of bias in the predictions of water and land allocation for years 2017 and 2018.

We found during our data assimilation experiments (not presented in this study) that the parameter ensembles are very sensitive to the uncertainty in some specific observations, especially observations of yield

elasticity ($\overline{\pi}_W$) and supply elasticity ($\overline{\eta}$). If the noise to signal ratio in the observations was too high, the ensemble of model parameters converged to a biased solution even if the observation errors were unbiased, and this is one contributor to the prediction biases. Kanellopoulos et al. (2010) did similar forecast experiments using two variants of the positive mathematical programming method and reported model prediction sensitivities to the supply elasticity parameters and biases in model forecasts.

Commonly, hydro-economic models of agricultural production that are calibrated using any standard variation of the PMP methodology are verified by reproducing the same baseline observations used for calibration. Model predictions under conditions different from those of the baseline are rarely verified with actual observations before the model is used in the simulation of design scenarios ((Graveline, 2016)). This is because the empirical nature of the positive mathematical programming method limits the application of models calibrated using this methodology to conditions that are not too different from those of the calibration. Our results show that the model has forecasting skill even under the unusual flash drought conditions of 2017 and can correctly reproduce the spatial patterns of land and water allocation at county scales, albeit with some biases. Further research is necessary to understand the range of conditions under which the model still provides valid forecasts.

A major strength of our model is its ability to track the hydrologic impact of producer behavior. In this demonstration we assumed that farmers can divert up to the maximum water diversions estimated over the calibration period. We did not explicitly incorporate water rights and other institutional or technological constraints that may limit agricultural water diversions in some parts of the state. These constraints, however, can partially be included by imposing a tighter limit on the total water available for irrigation. The results showed that the hydrologic impacts of agricultural activity are maximal in early and mid August, right before crops mature and water diversions start to decline. This is also the period of lowest natural flows, therefore agricultural water diversions can exacerbate ecological stress in streams during years of low summer flows. However, the simulations also show that the temporal impacts of diversions are circumscribed to the irrigation season and streamflows recover quickly after diversions cease due to contributions from the substantial groundwater available in many of Montana's watersheds. The simulations also show that diversions also have an extensive spatial impact and their impact propagates downstream from counties where irrigation is most prevalent, such as these at the headwaters of the Missouri, Gallatin, and Yellowstone rivers. This pattern is correctly captured by the model. However, downstream impacts do not propagate unabated, and the recovery of streams is clearly visible in some reaches downstream of diversion nodes (Figure 15. The recovery is caused by groundwater inflows into streams, which are known to be a key contributor to the resilience of riverine ecosystems in the region. Groundwater is not yet extensively used as a source of water for irrigation in the region, and this may be the reason why the impacts of agricultural diversions are limited in space and in time. Conjunctive management of surface and groundwater may therefore be desirable to maintain the strength and resilience of Montana's rivers.

The results from the hydrologic component presented earlier are only meant to illustrate the capabilities

of the coupled model and to provide a general view of the hydrologic impacts of agricultural activity in the region, but some model limitations need to be taken into account when interpreting modeled streamflows. For instance, this model demonstration assumed 70% efficiency in the water conveyance system and the irrigation technology for all counties and does not take into account water right limits. Although the assumption of constant irrigation efficiency is common (e.g. Elbakidze et al., 2012), this parameter varies between counties and years and can have an important impact on the actual timing of streamflows, and on the total volume of diverted water. Model refinements to improve the representation of these efficiencies are of major interest for state water managers and are underway. Another limitation of the current hydrologic component is that it does not yet include the effects of water impoundments. Artificial storage in dams and reservoirs and their release rules can have a large impact on the regional streamflow dynamics and provide additional resiliency by buffering and redistributing the spring freshet over a longer period. This model improvement is also a current priority.

7. Conclusions

Herein, we describe the implementation of a hydro-economic model composed of a stochastic economic model of agricultural production and a deterministic rainfall-runoff and streamflow routing model that explicitly represents the spatial configuration of the regional water distribution network. The spatially-explicit nature of the hydrologic model allows for tracking hydrologic impacts of producer activity. The economic component is designed to be continuously calibrated using remote sensing observations of land use, crop evapotranspiration, and crop production. The calibration method is based on an implementation of the PMP methodology within a data assimilation framework that permits recursive update of the model parameters when new remote sensing information becomes available. This new formulation of the calibration methodology eliminates some of the limitations that have previously hindered the use of hydro-economic models to inform agricultural water management over large regions and temporal extents (annual to multidecadal). Specifically, the model was designed to eliminate the need for expensive field surveys, reduce the problem of overfitting parameters to specific conditions of surveyed farms and years, and reduce the false sense of precision that is associated with fully deterministic models. We recognize the deterministic treatment of the hydrologic component as a current limitation of our modeling system. A stochastic hydrologic component is desirable to control the impact of hydroclimatic uncertainty on model predictions. Further work is necessary to make the modeling system fully stochastic without impairing it with an excessive computational burden.

We demonstrate the usefulness of the model in analyzing water use and agricultural production in the state of Montana. We show that satellite-based remote sensing retrievals of crop mix, land use allocations, water allocation and crop yield, and other ancillary information freely available online, contained sufficient information to correctly identify the parameters of the economic module. An interesting aspect of the recursive nature of the data assimilation methodology is that it allows analysis of the dynamics of the

other factors that drive decision-making and are hard to observe directly, such as declines in land fertility, existence of hidden production costs, etc. We calibrated the model with nine years of observations (2008-2016) and effectively reproduced the observed levels of resource allocation of the 2008 baseline year used to spin-up the parameters. The model also correctly predicted the spatial patterns of land and water allocation for years 2017 and 2018. Finally, we showed how the model can trace the effect of producer decision making on the regional hydrologic system. This innovation could be an important tool to better understand how producer behavior affects water availability in the future, and how agricultural water use at county scales propagates through the hydrologic system to impact downstream users. The analysis of the time and propagation of streamflow drawdowns induced by agricultural water use may also help identify regions that are at higher risk of water shortage during droughts.

The model was designed to address a number of essential questions related to understanding the vulnerability of agriculture to water shortage and the environmental impacts associated with agricultural development and on farm adaptation. In particular, we specifically built this model to address how farmers will reallocate land and water to mitigate loss of revenues under future climate projections and a range of water policy scenarios. For instance, the model can simulate the reaction and impact of water access restrictions (i.e., calls on senior water rights), potential changes in water delivery pricing, and/or of the effect of reducing farm operation costs through government incentives and subsidies. Simulated results can inform future policy options that promote agricultural adaptation and a more efficient use of the regional water resources.

References

Abatzoglou, J.T., 2013. Development of gridded surface meteorological data for ecological applications and modelling. International Journal of Climatology 33, 121–131. doi:10.1002/joc.3413.

Aerts, J.C.J.H., Botzen, W.J., Clarke, K.C., Cutter, S.L., Hall, J.W., Merz, B., Michel-Kerjan, E., Mysiak, J., Surminski, S., Kunreuther, H., 2018. Integrating human behaviour dynamics into flood disaster risk assessment. Nature Climate Change doi:10.1038/s41558-018-0085-1.

Allen, R.G., Tasumi, M., Trezza, R., 2007. Satellite-based energy balance for mapping evapotranspiration with internalized calibration (METRIC) - Model. Journal of Irrigation and Drainage Engineering-Asce 133, 380–394. doi:10.1061/(asce)0733-9437(2007)133:4(380).

Antle, J.M., Capalbo, S.M., 2001. Econometric-Process models for integrated assessment of agricultural production systems. American journal of agricultural economics 83, 389–401.

Arnade, C., Kelch, D., 2007. Estimation of area elasticities from a standard profit function. American journal of agricultural economics 89, 727–737.

Bergstrom, S., 1995. The HBV Model, in: Singh, V.P. (Ed.), Computer models of watershed hydrology.

Bergstrom, S., Forsman, A., 1973. Development of a conceptual deterministic rainfall-runoff model. Nordic hydrology doi:10.2166/nh.1973.013.

Brouwer, R., Hofkes, M., 2008. Integrated hydro-economic modelling: Approaches, key issues and future research directions. Ecological Economics 66, 16–22. doi:10.1016/j.ecolecon.2008.02.009.

Bryant, C.C.R., Smit, B., Brklacich, M., Johnston, T.R., Smithers, J., Chiotti, Q., Singh, B., 2000. Adaptation in Canadian agriculture to climatic variability and change. Climatic Change 45, 181–201. doi:10.1023/A:1005653320241.

Burt, O.R., Worthington, V.E., 1988. Wheat acreage supply response in the united states. Western Journal of Agricultural Economics 13, 100–111.

Cai, X., Ringler, C., caisub08 You, J.Y.L.B., 2008. Substitution between water and other agricultural inputs: Implications for water conservation in a River Basin context. Ecological Economics 66, 38–50.

Cai, X.M., Rosegrant, M.W., Ringler, C., 2003. Physical and economic efficiency of water use in the river basin: Implications for efficient water management. Water Resources Research 39.

Chavas, J.P., Holt, M.T., 1990. Acreage decisions under risk: The case of corn and soybeans. American journal of agricultural economics 72, 529–538.

Chembezi, D.M., Womack, A.W., 1992. Regional acreage response for US corn and wheat: the effects of government programs. Journal of Applied Agricultural Economics 24, 187–198.

Chow, V.T., M.D., Mays, L., 1988. Applied hydrology. McGraw-Hill, New York.

Cobourn, K., Crescenti, N., 2011. The implications of surface-groundwater hydrology for optimal conjunctive management. Western Economics Forum 10.

Connell-Buck, C.R., Medellín-Azuara, J., Lund, J.R., Madani, K., 2011. Adapting California's water system to warm vs. dry climates. Climatic Change 109, 133–149. doi:10.1007/s10584-011-0302-7.

Cunge, J.A., 1969. On the subject of a flood propagation computation method (musklngum method). Journal of Hydraulic Research doi:10.1080/00221686909500264.

Department of Water Resources, 2009. California Water Plan Update. Technical Report. California Department of Water Resources. Sacramento, California.

Driessen, T.L., Hurkmans, R.T., Terink, W., Hazenberg, P., Torfs, P.J., Uijlenhoet, R., 2010. The hydrological response of the Ourthe catchment to climate change as modelled by the HBV model. Hydrology and Earth System Sciences doi:10.5194/hess-14-651-2010.

Easterling, D.R., Evans, J.L., Groisman, P.Y., Karl, T.R., Kunkel, K.E., Ambenje, P., 2000. Observed Variability and Trends in Extreme Climate Events: A Brief Review*. Bulletin of the American Meteorological Society 81, 417–425. doi:doi:10.1175/1520-0477(2000)081<0417:OVATIE>2.3.CO;2.

Elbakidze, L., Shen, X., Taylor, G., Mooney, S., 2012. Spatiotemporal analysis of prior appropriations water calls. Water Resources Research doi:10.1029/2011WR010609.

Elbakidze, L., Vinson, H., Cobourn, K., Taylor, R.G., 2018. Efficient groundwater allocation and binding hydrologic externalities. Resource and Energy Economics doi:10.1016/j.reseneeco.2018.05.002.

Evensen, G., 1994. Sequential data assimilation with a nonlinear quasi-geostrophic model using Monte Carlo methods to forecast error statistics. J. Geophys. Res. 99, 10,110–143,162.

Garnache, C., Mérel, P., Howitt, R., Lee, J., 2017. Calibration of shadow values in constrained optimisation models of agricultural supply. European Review of Agricultural Economics doi:10.1093/erae/jbx005.

George H. Hargreaves, Zohrab A. Samani, 1985. Reference Crop Evapotranspiration from Temperature. Applied Engineering in Agriculture doi:10.13031/2013.26773.

Ghosh, S., Coburn, K.M., Elbakidze, L., 2014. Water banking, conjunctive administration, and drought: The interaction of water markets and prior appropriation in southeastern Idaho. Water Resources Research , 6927–6949doi:10.1002/2014WR015572.Received.

Gorelick, S.M., Zheng, C., 2015. Global change and the groundwater management challenge. Water Resources Research doi:10.1002/2014WR016825.

Graveline, N., 2016. Economic calibrated models for water allocation in agricultural production : a review. Environmental Modelling and Software 81, 12–25. doi:10.1016/j.envsoft.2016.03.004.

Graveline, N., Merel, P., 2014. Intensive and extensive margin adjustments to water scarcity in France's cereal belt. European Review of Agricultural Economics 41, 707–743. doi:https://doi.org/10.1093/erae/jbt039.

Groisman, P.Y., Easterling, D.R., 1994. Variability and Trends of Total Precipitation and Snowfall over the United States and Canada. Journal of Climate 7, 184–205. doi:10.1175/1520-0442(1994)007<0184:VATOTP>2.0.CO;2.

Harou, J., Medellin, J., Zhu, T., Tanaka, S., Lund, J., Stine, S., Jenkins, M., Olivares, M., 2006. Extreme Drought and Water Supply Management in California, in: Randall, G. (Ed.), ASCE World Environmental and Water Resources Institute Congress 2006, ASCE, Omaha, Nebraska. p. 278.

Harou, J.J., Pulido-Velazquez, M., Rosenberg, D.E., Medellín-Azuara, J., Lund, J.R., Howitt, R.E., 2009. Hydro-economic models: Concepts, design, applications, and future prospects. Journal of Hydrology 375,

He, M., Kimball, J.S., Yi, Y., Running, S.W., Guan, K., Moreno, A., Wu, X., Maneta, M., 2019. Satellite data-driven modeling of field scale evapotranspiration in croplands using the MOD16 algorithm framework. Remote Sensing of Environment 230, 111201. doi:10.1016/j.rse.2019.05.020.

He, M., Kimball, J.S.J., Maneta, M.P.M., Maxwell, B.D.B., Moreno, A., Beguería, S., Wu, X., 2018. Regional crop gross primary productivity and yield estimation using fused landsat-MODIS data. Remote Sensing 10. doi:10.3390/rs10030372.

Heckelei, T., Britz, W., Zhang, Y., 2012. Positive Mathematical Programming Approaches – Recent Developments in Literature and Applied Modelling. Bio-based and applied economics 1, 109–124.

Hendricks, N.P., Smith, A., Sumner, D.A., 2014. Crop supply dynamics and the illusion of partial adjustment. American journal of agricultural economics 96, 1469–1491.

Howitt, R.E., 1995. Positive mathematical programming. American Journal of Agricultural Economics 77, 329–342.

Howitt, R.E., Medellín-Azuara, J., MacEwan, D., Lund, J.R., 2012a. Calibrating disaggregate economic models of agricultural production and water management. Environmental Modelling & Software 38, 244–258. doi:10.1016/j.envsoft.2012.06.013.

Howitt, R.E., Medellín-Azuara, J., MacEwan, D., Lund, J.R., 2012b. Calibrating disaggregate economic models of agricultural production and water management. Environmental Modelling & Software 38, 244–258.

Kahil, M.T., Ward, F.A., Albiac, J.M., Eggleston, J., Sanz, D., 2015. Hydro-economic modeling with aquifer-river interactions to guide sustainable basin management. Journal of Hydrology 539, 510–524. doi:10.1016/j.jhydrol.2016.05.057.

Kanellopoulos, A., Berentsen, P., Heckelei, T., van Ittersum, M., Lansink, A.O., 2010. Assessing the forecasting performance of a generic bio-economic farm model calibrated with two different PMP variants. Journal of Agricultural Economics 61, 274–294. doi:10.1111/j.1477-9552.2010.00241.x.

Kimball, J.S., Jones, L., Jencso, K., He, M., Maneta, M., Reichle, R., 2019. SMAP L4 Assessment of the U.S. Northern Plains 2017 Flash Drought, in: International Geoscience and Remote Sensing Symposium (IGARSS). doi:10.1109/IGARSS.2019.8898354.

Knapp, K.C., . ECONOMIC FACTORS AFFECTING THE CALIFORNIA ALFALFA MARKET. alfalfa.ucdavis.edu .

Lee, D.R., Helmberger, P.G., 1985. Estimating supply response in the presence of farm programs. American journal of agricultural economics 67, 193–203.

Lin, W., Dismukes, R., 2007. Supply response under risk: Implications for Counter-Cyclical payments' production impact. Applied Economic Perspectives and Policy 29, 64–86.

Lindström, G., Johansson, B., Persson, M., Gardelin, M., Bergström, S., 1997. Development and test of the distributed HBV-96 hydrological model. Journal of Hydrology doi:10.1016/S0022-1694(97)00041-3.

Long, D., Scanlon, B.R., Longuevergne, L., Sun, A.Y., Fernando, D.N., Save, H., 2013. GRACE satellite monitoring of large depletion in water storage in response to the 2011 drought in Texas. Geophysical Research Letters 40, 3395–3401. doi:10.1002/grl.50655.

Maneta, M.P., Torres, M., Vosti, S.S.A., Wallender, W.W., Allen, S., Bassoi, L.H.L.L.H., Bennett, L., Howitt, R., Rodrigues, L., Young, J., 2009a. Assessing agriculture–water links at the basin scale: hydrologic and economic models of the São Francisco River Basin, Brazil. Water International 34, 88 – 103. doi:10.1080/02508060802669496.

Maneta, M.P., Torres, M.O., Wallender, W.W., Vosti, S., Howitt, R.E., Rodrigues, L., Bassoi, L.H., Panday, S., 2009b. A spatially distributed hydroeconomic model to assess the effects of drought on land use, farm profits, and agricultural employment. Water Resour. Res. 45, W11412. doi:10.1029/2008wr007534.

Maneta, M.P.M., Howitt, R.E., 2014. Stochastic calibration and learning in non-stationary hydro-economic models. Water Resources Research 50, 3976–3993. doi:10.1002/2013WR015196.

McCabe, G., Clark, M., 2005. Trends and Variability in Snowmelt Runoff in the Western United States. Journal of Hydrometeorology 6, 476–482. doi:doi:10.1175/JHM428.1.

McCarl, A.B., 2015. Elaborations on climate adaptation in U.S. agriculture. Choices 30, 1–5.

Medellín-Azuara, J., Harou, J.J., Olivares, M.A., Madani, K., Lund, J.R., Howitt, R.E., Tanaka, S.K., Jenkins, M.W., 2008. Adaptability and Adaptations of California's Water Supply System to Dry Climate Warming. Climatic Change 87, S75–S90.

Medellín-Azuara, J., Howitt, R., Lund, J.R., 2011. Hydro-economic modeling to assess climate impact and adaptation for agriculture in California, in: Dinar, A., Mendelsohn, R. (Eds.), Handbook on Climate Change and Agriculture. Edward Elgar. chapter 15, p. Chapter 15.

Menzel, A., von Vopelius, J., Estrella, N., Schleip, C., Dose, V., 2006. Farmers' annual activities are not tracking the speed of climate change. Climate Research 32, 201–207.

Menzel, L., Bürger, G., 2002. Climate change scenarios and runoff response in the Mulde catchment (Southern Elbe, Germany). Journal of Hydrology doi:10.1016/S0022-1694(02)00139-7.

Mérel, P., Simon, L.K., Yi, F., 2011. A fully calibrated generalized constant-elasticity-of-substitution programming model of agricultural supply. American Journal of Agricultural Economics 93, 936–948.

Mérel, P., Yi, F., Lee, J., Six, J., 2014. A regional bio-economic model of nitrogen use in cropping. American Journal of Agricultural Economics 96, 67–91.

Miao, R., Khanna, M., Huang, H., 2016. Responsiveness of Crop Yield and Acreage to Prices and Climate. American Journal of Agricultural Economics 98, 191–211. doi:10.1093/ajae/aav025.

Mote, P., 2006. Climate-driven variability and trends in mountain snowpack in western North America. Journal of Climate 19, 6209–6220.

Mu, Q., Jones, L.A., Kimball, J.S., McDonald, K.C., Running, S.W., 2009. Satellite assessment of land surface evapotranspiration for the pan-Arctic domain. Water Resources Research 45, n/a–n/a. doi:10.1029/2008WR007189.

Mu, Q., Zhao, M., Running, S.W., 2011. Improvements to a MODIS global terrestrial evapotranspiration algorithm. Remote Sensing of Environment 115, 1781–1800. doi:10.1016/j.rse.2011.02.019.

National atlas of the United States, 2014. Forest Cover Types. Reston, VA.

Ng, T.L., Eheart, J.W., Cai, X., Braden, J.B., 2011. An agent-based model of farmer decision-making and water quality impacts at the watershed scale under markets for carbon allowances and a second-generation biofuel crop. Water Resources Research 47. doi:10.1029/2011WR010399.

Oehmke, J.F., Yao, X., 1990. A policy preference function for government intervention in the US wheat market. American journal of agricultural economics 72, 631–640.

Pulido-Velazquez, M., Jenkins, M.W., Lund, J.R., . Economic values for conjunctive use and water banking in southern California. Water Resources Research 40.

Rose, S., 2015. The inevitability of climate adaptation in U.S. agriculture. Choices 30, 1–5.

Schneider, S.H., Easterling, W.E., Mearns, L.O., 2000. Adaptation: Sensitivity to Natural Variability, Agent Assumptions and Dynamic Climate Changes. Climatic Change 45, 203–221. doi:10.1023/A:1005657421149.

Sullivan, J., Wainio, J., Roningen, V., 1989. A Database for Trade Liberalization Studies. U.S. Department of Agriculture, Economic Research Service, Agriculture and Trade Analysis Division.

Torres, M.d.O., Maneta, M., Howitt, R., Vosti, S.A., Wallender, W.W., Bassoi, L.H., Rodrigues, L.N., 2011. Economic impacts of regional water scarcity in the São Francisco River Basin, Brazil: an application of a linked hydro-economic model. Environment and Development Economics 21, 1–22. doi:doi:10.1017/S1355770X11000362.

US Army Corps of Engineers, US Army Corps of Engineers, 2012. Water in the U.S. American West: 150

US Bureau of Reclamation, 2011. North of Delta Offstream Storage (NODOS) Analysis and SWAP model Application to Natinal Economic Development (NED). Technical Report. Mid-Pacific Region. Sacramento, California.

USDA NASS, 2015. Cropland data layer. Published crop-specific data layer [Online], USDA-NASS. Washington, DC. URL: Availableathttps://nassgeodata.gmu.edu/CropScape/.

Ward, F.A., Booker, J.F., Michelsen, A.M., 2006. Integrated Economic , Hydrologic , and Institutional Analysis of Policy Responses to Mitigate Drought Impacts in Rio Grande Basin. Journal of Water Resources Planning and Management 132, 488–502.

Ward, F.A., Lynch, T.P., 1996. Integrated river basin optimization: Modeling economic and hydrologic interdependence. Water Resources Bulletin 32, 1127–1138.

Weersink, A., Jeffrey, S., Pannell, D., 2002. Farm-Level Modeling for Bigger Issues. Applied Economic Perspectives and Policy 24, 123–140. doi:10.1111/1058-7195.00009.

Wens, M., Johnson, J.M., Zagaria, C., Veldkamp, T.I.E., 2019. Integrating human behavior dynamics into drought risk assessment—A sociohydrologic, agent-based approach. Wiley Interdisciplinary Reviews: Water doi:10.1002/wat2.1345.

West, M., 1993. Mixture models, Monte Carlo, Bayesian updating and dynamic models. Computing Science and Statistics 25, 325–333.

White, J.W., Hoogenboom, G., Kimball, B.A., Wall, G.W., 2011. Methodologies for simulating impacts of climate change on crop production. Field Crops Research 124, 357–368. doi:10.1016/j.fcr.2011.07.001.

Whitlock, C., Cross, W., Maxwell, B., Silverman, N., Wade, A., 2017. Montana Climate Assessment. Technical Report. Institute on Ecosystems. Bozeman and Missoula, MT. doi:10.15788/m2ww8w.

Wurster, P.M., Maneta, M., Begueria, S., Cobourn, K., Maxwell, B., Silverman, N., Ewing, S., Jensco, K., Gardner, P., Kimball, J., Holden, Z., Vicente-Serrano, S.M., 2019. Characterizing the impact of climatic anomalies on agrosystems in the northwest United States. Agricultural and Forest Meteorology 280. doi:10.1016/j.agrformet.2019.107778.

Zhang, K., Kimball, J.S., Nemani, R.R., Running, S.W., 2010. A continuous satellite-derived global record of land surface evapotranspiration from 1983 to 2006. Water Resources Research 46. doi:10.1029/2009WR008800.

Appendix A. Hydrologic model

The hydrologic system is simulated using a rainfall-runoff model coupled to a routing component that sim-

and Forsman, 1973) to simulate subcatchment-scale hydrologic processes (snowmelt, evapotranspiration, infiltration) and to transform precipitation into runoff and streamflow. Runoff that reaches the channel is routed through the stream network using the Muskingum-Cunge routing algorithm Chow and Mays (1988). In this appendix we provide here a description of the implementation of the algorithms.

Appendix A.1. Rainfall Runoff component

The HVB model (Bergstrom, 1995; Bergstrom and Forsman, 1973) is implemented as a mixture of gridded and vector-based operations to leverage the distributed nature of raster meteorological datasets while simultaneously taking advantage of the reduced computational burden of operating over polygons that aggregate runoff production over uniform hydrologic response units (HRUs).

Snowpack accumulation and melt and soil processes are calculated over the uniform raster grid imposed by the meteorological inputs (precipitation, air temperature, and potential evapotranspiration). In the next two paragraphs subscript i indicates that the variable or parameter is spatially distributed and is represented at grid point i. Superscript t indicates that the variable is dynamic and its value is represented at time step t. Variables with no script or superscript indicate that the variable is spatially constant or time invariant.

Precipitation and snowpack processes. Precipitation is partitioned between snowfall and rainfall using minimum and maximum daily air temperatures and a critical temperature threshold Tc that determines the the snow-rain transition:

$$Snow_i^t = \begin{cases} P_i^t & Tmax_i^t < Tc_i \\ P_i^t * \frac{Tc_i - Tmin_i^t}{Tmax_i^t - Tmin_i^t} & Tmin_i^t < Tc_i < Tmax_i^t \\ 0 & Tmin_i^t > Tc_i \end{cases} \tag{A.1}$$

$$Rain_i^t = P_i^t - Snow_i^t \tag{A.2}$$

where P is precipitation ($\mathrm{mm\,d^{-1}}$), T_{max} and T_{min} are maximum and minimum air temperature (°C), $Rain$ is liquid precipitation and $Snow$ is snowfall at pixel i during time step t ($\mathrm{mm\,d^{-1}}$). Snowfall during day t contributes to the snow water equivalent (SWE, (mm)) of the snowpack:

$$SWE_i^t = SWE_i^{t-1} + Snow_i^t \Delta t \tag{A.3}$$

The snowpack melt process is simulated using a degree day factor model occurs when average air temperature exceeds a air temperature threshold (Tm):

$$Melt_i^t = ddf_i * (Tav_i^t - Tm_i)] \text{ for } Tav_i^t > Tm_i \tag{A.4}$$

$$Rain_i^t = P_i^t - Snow_i^t \tag{A.5}$$

where $Melt$ is the amount of water output from the snowpack ($\mathrm{mm\,d^{-1}}$), Tav is average air temperature over the time step (°C), and ddf is the degree day factor ($\mathrm{mm\,d^{-1}\,°C^{-1}}$), an empirical parameter that represents the snowmelt rate per degree of air temperature above Tm. Any melt form the snowpack during time t is subtracted from the snowpack storage (SWE) and added to the amount of water ponded in the surface:

$$Pond_i^t = Pond_i^{t-1} + (Melt_i^t + Rain_i^t)\Delta t \tag{A.6}$$

$$SWE_i^t = SWE_i^t - Melt_i^t \Delta t \tag{A.7}$$

where $Pond$ (mm) is liquid water available on the surface to infiltrate or produce runoff.

Soil processes. Recharge into the soil system occurs when liquid water ponding the surface infiltrates into the soil. Ponded water that is not infiltrated increases the topsoil compartment that generates fast runoff. The fraction of ponded water that infiltrates into the soil is a exponential function of the relative water storage in the soil:

$$\Delta SM_i^t = Pond_i^t * \left(1 - \frac{SM_i^t}{FC_i^t}\right)^{\beta} \tag{A.8}$$

$$\tag{A.9}$$

where SM (mm) is the amount of water in the soil compartment, FC (mm) is the maximum amount of water soil can hold before water starts percolating to the groundwater system, and $beta$ (dimensionless) is an empirical parameter. Simultaneously, actual evapotranspiration (AET, $\mathrm{mm\,d^{-1}}$) reduces the amount of water storage in the soil and is also controlled by the degree of saturation of the soil (ration of SM to FC).

$$AET_i^t = PET_i^t * \left(\frac{SM_i^t}{FC_i * LP_i}\right)^{l} \tag{A.10}$$

$$\tag{A.11}$$

where PET is potential evapotranspiration ($\mathrm{mm\,d^{-1}}$)) and l is an empirical dimensionless parameter. Infiltration and actual evapotranspiration control the dynamics of water storage in the soil and amount of surface water that generates fast runoff:

$$SM_i^t = SM_i^t + \Delta SM_i^t - AET_i^t \Delta t \tag{A.12}$$

$$OVL_i^t = Pond_i^t - \Delta SM_i^t \tag{A.13}$$

where OVL (mm) is water that recharges the upper (near-surface) runoff-generating compartment.

Percolation and runoff generation. Excess water in the topsoil and in two groundwater compartments generate outflow that represent fast and intermediate runoff and baseflow. These processes are implemented at the HRU level. For this, calculations about overland flow generation and soil moisture performed at the grid level are averaged over subwatersheds representing HRUs. Spatial arithmetic averaging soil water storage over all grid cells i contained within a given HRU j is represented using angle brackets $< . >$. The mass balance and percolation of water from the soil upper to the soil lower zone is implemented as:

$$Rech_j^t =< OVL_i^t >_j + < max(SM_i^t - FC_i, 0) >_j \tag{A.14}$$

$$SUZ_j^t = SUZ_j^{t-1} + Rech_j^t + Pond_j^t - Q0_j^t \Delta t - Q1_j \Delta t - PERC_j \tag{A.15}$$

$$SLZ_j^t = SLZ_j^{t-1} + PERC_j - Q2\Delta t \tag{A.16}$$

$Rech$ (mm) is water storage in the near-surface compartment that generates fast runoff, SUZ (mm) is the storage in the upper groundwater compartment, and SLZ (mm) is water storage in the lower (deeper) groundwater compartment in HRU j at time step t. Q_0, Q_1, and Q_2 (mm d^{-1}) are specific runoff rates from the soil surface, and the upper and lower soil zones:

$$Q0_j^t = max((SUZ_j - HL1_j) * \frac{1}{CK0_j}, 0.0) \tag{A.17}$$

$$Q1_j^t = SUZ_j * \frac{1}{CK1_j} \tag{A.18}$$

$$Q2_j^t = SLZ_j * \frac{1}{CK2_j} \tag{A.19}$$

$$Qall_j^t = Q0_j^t + Q1_j^t + Q2_j^t \tag{A.20}$$

where $HL1$ (mm) is an empirical water storage threshold the triggers the generation of fast runoff, and $CK0$, $C10$, $CK2$ (d) are empirical parameters representing the characteristic drainage time of each of the compartments. Total outflow from HRU j on day t is distributed over time to produce the catchment response by convoluting the output of HRU j by triangular standard unit hydrograph with base M_{base}.

$$Q_j^t = \sum_{i=1}^{M_{base}} Qall_j^{t-i+1} U(i) \tag{A.21}$$

$$U(i) = \begin{cases} \frac{4}{M_{base}^2} * i & 0 < i < M_{base}/2 \\ -\frac{4}{M_{base}^2} * i + \frac{4}{M_{base}} & M_{base}/2 < i < M_{base} \end{cases} \tag{A.22}$$

where U is a triangular hydrograph of area 1 and a base $MAXBAS$ (d)representing the hydrograph duration

.

Appendix A.2. Routing component

The response at the end of each HRU is routed through the stream network using the Muskingum-Cunge

equation:

$$S_k^t = K\left[eQ_{in} + (1-e)Q_{out}\right], \tag{A.23}$$

which has parameters K (d) and e (dimensionless) controlling, respectively, the celerity and dispersion of the wave routed through the channel.

Substituting this relationship in a finite-difference form of the continuity equation $\frac{S_j^{t+1}-S_j^t}{\Delta t} = Q_{in} - Q_{out}$ for a multi-reach system with lateral inflows injected upstream of reach draining $HRU\ j$ at average constant rate through time step t q_j^{t+1} yields:

$$Q_j^{t+1}\left[K_j(1-e_j) + 0.5\Delta t\right] + Q_{j-1}^{t+1}\left[K_j e_j - 0.5\Delta t\right] \tag{A.24}$$

$$= Q_j^t\left[K_j(1-e_j) - 0.5\Delta t\right] + Q_{j-1}^t\left[K_j e_j + 0.5\Delta t\right] \tag{A.25}$$

$$+ q_j^{t+1}\left[K_j(1-e_j) + 0.5\Delta t\right] \tag{A.26}$$

Each of the $HRUs$ contains one reach with an upstream and a downstream node. Streamflows for each of the $j = 1, ..., J$ reaches are integrated over time using a first-order explicit finite difference scheme. The system of J equations can be assembled as a linear system of the form:

$$\mathbf{A}\mathbf{Q}^{\mathbf{t+1}} = \mathbf{B} \tag{A.27}$$

where $\mathbf{Q}^{\mathbf{t+1}}$ is the vector of unknown streamflows at time $t+1$ for each of the J reaches of the network that is solved each time step. Matrices $\mathbf{A}$ add $\mathbf{B}$ are functions of the model parameters and streamflows at timestep t:

$$\mathbf{A} \equiv (\mathbf{a} + \mathbf{\Phi b})^T \tag{A.28}$$

$$\mathbf{B} \equiv (\mathbf{d} + \mathbf{\Phi c})^T\mathbf{Q}^t + \mathbf{I}(\mathbf{a} \odot \mathbf{q}^{t+1}) \tag{A.29}$$

where $\mathbf{\Phi}$ is a JxJ sparse connectivity (0,1)-matrix where the elements indicate if two pairs of nodes are connected. Flow direction is from nodes in the rows to nodes in the columns. Rows representing the upstream node of $HRUs$ that drain an outlet node (exit the domain) are all zero. Finally,

$$\mathbf{a} = \mathbf{I}(\mathbf{K} - \mathbf{K} \odot \mathbf{e}) + dt * 0.5 \tag{A.30}$$

$$\mathbf{b} = \mathbf{I}(\mathbf{K} \odot \mathbf{e}) - dt * 0.5 \tag{A.31}$$

$$\mathbf{c} = \mathbf{I}(\mathbf{K} - \mathbf{K} \odot \mathbf{e}) - dt * 0.5) \tag{A.32}$$

$$\mathbf{d} = \mathbf{I}(\mathbf{K} \odot \mathbf{e}) + dt * 0.5 \tag{A.33}$$

where $\mathbf{K}$ is the identity matrix of order J, $\mathbf{K}$ and $\mathbf{e}$ are column vectors holding parameters K and e for each of the N reaches in the network. The $\odot$ operator denotes the Schur (elementwise) product between two vectors. The solution of (A.27) becomes unstable if $\Delta t > 2 * K_j * (1 - e_j)$. To ensure robust and stable solution an adaptive time stepping scheme was implemented. In this scheme, the default time step is reduced by an integer fraction until the the stability condition is satisfied in all reaches.

Appendix B. Economic model

Here we briefly outline the economic optimization program using the standard Positive Mathematical Programming (PMP), following Howitt (1995); Mérel et al. (2011) and Garnache et al. (2017). The economic program is implemented in two step: in the first step, parameters for the economic model are calibrated such that the program mimics the observed land and water use decisions. In the second step, the model simulates farmer's land use and water use responses given these model parameters along with other exogenous factors such as availability of supplemental irrigation water. The following subsections briefly outline the calibration and the simulation process at each simulation time.

Appendix B.1. Calibration

The fundamental aspect of our economic program is that farmers allocate resources with the objective of maximizing net revenues, where the revenue function follows a generalized constant elasticity of substitution (CES) functional form:

$$\begin{aligned}
\max_{x_{land,i}, x_{water,i}} \quad & \sum_i \Bigg\{ p_i \mu_i \left[\beta_{land,i} x_{land,i}^{\rho_i} + \beta_{water,i} (x_{precip,i} + x_{water,i})^{\rho_i} \right]^{\frac{\delta_i}{\rho_i}} \\
& - (c_{land,i} + \lambda_{land,i}) \, x_{land,i} - (c_{water,i} + \lambda_{water,i}) \, x_{water,i} \Bigg\} \\
\text{subject to} \quad & \sum_i x_{land,i} \leq \overline{L} \left[\overline{\lambda}_{land} \right] \\
& \sum_i x_{water,i} \leq \overline{W} \left[\overline{\lambda}_{water} \right] \\
& x_{land,i}, x_{water,i} \geq 0
\end{aligned} \tag{B.1}$$

where $i = 1, ..., I$ indexes crops; $l = land, water$ indexes land and water inputs. We differentiate water inputs into an exogenous component $x_{precip,i}$, which captures water provided by natural sources like precipitation, and an endogenous component $x_{water,i}$, which captures supplemental irrigation water provision. Total water application will be the summation of the two, i.e.

$$x^*_{water,i} \equiv x_{precip,i} + x_{water,i}$$

The unknown parameters in Equation B.1 are $\mu_i, \beta_{il}, \rho_i, \delta_i, \lambda_{il}, \overline{\lambda}_1$; and the known values are:

- $\overline{\pi}_i$: observed crop production for crop i
- $\overline{x}_{land,i}$: observed land allocation for crop i
- $\overline{x}^*_{water,i}$: observed ET (total) for crop i
- $\overline{y}_{iW}$: reference yield elasticity with respect to water for crop i (% change in production over % change in total ET)
- σ_i: elasticity of substitution for crop i
- p_i: unit price of crop i
- c_{il}: per-unit input costs of production for crop i, input l
- $\overline{L}$: total arable land
- $\overline{W}$: total amount of supplemental irrigation water available

Given the above maximization problem, the unknown parameters can be calibrated via positive mathematical programming, using the following set of calibration equations:

$$
\begin{aligned}
&\rho_i = \frac{\sigma_i - 1}{\sigma_i} \text{ for } i = 1, \ldots, I \\
&\overline{\eta}_i = \frac{\delta_i}{1-\delta_i}\left\{1 - \frac{\frac{b_i}{\delta_i(1-\delta_i)}}{\sum_j\left[\frac{b_j}{\delta_j(1-\delta_j)} + \frac{\sigma_j b_j \overline{y}_{jW}}{\delta_j\left(\delta_j - \overline{y}_{jW}\right)}\right]}\right\} \text{ for } i = 1, \ldots, I, \text{where } b_i = \frac{\overline{x}^2_{land,i}}{p_i \overline{\pi}_i} \\
&\overline{\pi}_{iW} = \delta_i\left(\frac{\beta_{water,i}\overline{x}^{*\rho_i}_{water,i}}{\beta_{land,i}\overline{x}^{\rho_i}_{land,i} + \beta_{water,i}\overline{x}^{*}_{water,i}\rho_i}\right) \text{ for } i = 1, \ldots, I \\
&\beta_{land,i} + \beta_{water,i} = 1 \text{ for } i = 1, \ldots, I \\
&\overline{\pi}_i = \mu_i\left[\beta_{land,i}\overline{x}^{\rho_i}_{land,i} + \beta_{water,i}\overline{x}^{*\rho_i}_{water,i}\right]^{\frac{\delta_i}{\rho_i}} \text{ for } i = 1, \ldots, I \\
&\overline{\lambda}_1 = \frac{\sum_i \left[p_i\overline{\pi}_i\left(\delta_i - \overline{y}_{iW}\right) - c_{land,i}\overline{x}_{land,i}\right]\overline{x}_{land,i}}{\sum_i\left(\overline{x}^2_{land,i}\right)} \\
&p_i\overline{\pi}_i\left(\delta_i - \overline{y}_{iW}\right) = \left(c_{land,i} + \lambda_{land,i} + \overline{\lambda}_1\right)\overline{x}_{land,i} \text{ for } i = 1, \ldots, I \\
&p_i\overline{\pi}_i\overline{y}_{iW} = \left(c_{water,i} + \lambda_{water,i}\right)\overline{x}^*_{water,i} \text{ for } i = 1, \ldots, I
\end{aligned}
\tag{B.2}
$$

Appendix B.2. Simulation

After calibrating the model parameters, the optimization framework can now be used to analyze how farmer behaviors will change given changes in exogenous environmental and economic factors, including water availability, crop prices, and production costs.

The simulation problem is given by the following maximization problem:

$$\begin{aligned}
\max_{x_{land,i},x_{water,i}} \sum_i \Bigg\{ & p_i \mu_i \left[\beta_{land,i} x_{land,i}^{\rho_i} + \beta_{water,i} x_{water,i}^{*\rho_i} \right]^{\frac{\delta_i}{\rho_i}} \\
& - \left(c_{land,i} + \lambda_{land,i} \right) x_{land,i} - \left(c_{water,i} + \lambda_{water,i} \right) x_{water,i} \Bigg\} \\
\text{subject to } & \sum_i x_{land,i} \leq \overline{L} \left[\overline{\lambda}_{land} \right] \\
& \sum_i x_{water,i}^{*} \leq \overline{W} \left[\overline{\lambda}_{water} \right] \\
& \text{and } x_{water,i} \geq 0 \left[\xi_i \right]
\end{aligned} \tag{B.3}$$

where the unknown values are $x_{land,i}, x_{water,i}$, the land and water inputs for crop i; π_i, the total production for crop i; and $\overline{\lambda}_{land}, \overline{\lambda}_{water}, \xi$, the Lagrangian multipliers. The known values include:

- $\mu_i, \beta_{il}, \rho_i, \delta_i, \lambda_{il}$: model parameters determined from the calibration equations
- $p_i, c_{il}, x_{precip,i}, \overline{L}, \overline{W}$: crop prices, per unit production costs, water from natural sources, total arable land, and total supplemental irrigation water (same as in the calibration equation B.1).

The simulation equations to solve the above maximization problem are given by:

$$\begin{aligned}
& \frac{p_i \delta_i \pi_i \beta_{land,i} x_{land,i}^{\rho_i}}{\beta_{land,i} x_{land,i} \rho_i + \beta_{water,i} x_{water,i}^{*\rho_i}} = \left(c_{land,i} + \lambda_{land,i} + \lambda_1 \right) x_{land,i} \text{ for } i = 1, \ldots, I \\
& \frac{p_i \delta_i \pi_i \beta_{water,i} x_{water,i}^{*\rho_i}}{\beta_{land,i} x_{land,i}^{\rho_i} + \beta_{water,i} x_{water,i}^{*} \rho_i} = \left(c_{water,i} + \lambda_{water,i} + \lambda_2 + \xi_i \right) x_{water,i}^{*} \text{ for } i = 1, \ldots, I \\
& \pi_i = \mu_i \left[\beta_{land,i} x_{land,i}^{\rho_i} + \beta_{water,i} x_{water,i}^{*\rho_i} \right]^{\frac{\delta_i}{\rho_i}} \text{ for } i = 1, \ldots, I \\
& \sum_i x_{land,i} = \overline{L} \text{ for } i = 1, \ldots, I \\
& \sum_i x_{water,i}^{*} = \overline{W} \text{ for } i = 1, \ldots, I
\end{aligned} \tag{B.4}$$

The simulation model will be able to recover farmers land and water use choices, $x_{land,i}$ and $x_{water,i}$, under the new set of exogenous conditions. The model will also be able to recover shadow values with respect to land and water inputs, $\overline{\lambda}_{land}$ and $\overline{\lambda}_{water}$.

Note that this system of equations requires that the water constraint is binding. If the water constraint is non-binding, complementary slackness conditions need to be built to allow for the case in which $\lambda_{water} = 0$.

Appendix C. Appendix Tables

Table A1: Supply elasticity estimates

Authors	Journal	Region	Elasticity
Alfalfa			
Howitt et al. (2012b)	Env Mod Softw	California	0.44
Knapp	Working Paper	California	0.61
Author's Calculation			0.141
Barley			
Antle and Capalbo (2001)	Am J. Ag Econ	Northern Plains	0.35
Authors' Calculation			-0.408 (dropped)
Maize			
Hendricks et al. (2014)	Am J. Ag Econ	Iowa, Illinois, Indiana	0.40 (short run)
Hendricks et al. (2014)	Am J. Ag Econ	Iowa, Illinois, Indiana	0.29 (long run)
Arnade and Kelch (2007)	Am J. Ag Econ	Iowa	0.2
Lin and Dismukes (2007)	Rev. Ag Econ	North Central Region	0.17 (linear model)
Lin and Dismukes (2007)	Rev. Ag Econ	North Central Region	0.35 (acreage share model)
Miao et al. (2016)	Am J. Ag Econ	United States	0.68
Chavas and Holt (1990)	Am J. Ag Econ	North Central Region	0.15
Howitt et al. (2012b)	Env Mod Softw	California	0.55
Chembezi and Womack (1992)	J. Ag Applied Econ	United States	0.1
Lee and Helmberger (1985)	Am J. Ag Econ	United States	0.05
Houck & Gallagher (1976)	Am J. Ag Econ	United States	0.24 (lower bound)
Houck & Gallagher (1976)	Am J. Ag Econ	United States	0.76 (upper bound)
Authors' Calculation[a]			0.762
Wheat			
Antle and Capalbo (2001)	Am J. Ag Econ	Northern Plains	0.36 (winter wheat)
Antle and Capalbo (2001)	Am J. Ag Econ	Northern Plains	0.14 (spring wheat)
Burt and Worthington (1988)	J Ag Res Econ	Great Plains	1.5
Howitt et al. (2012b)	Environ. Model. Softw	California	0.36
Oehmke and Yao (1990)	Am J. Ag Econ	US	0.4
Sullivan et al. (1989)	USDA report	US	0.5
Authors' Calculation			0.368 (winter wheat)
Authors' Calculation			0.409 (spring wheat)

[a] We empirically calculate the supply elasticity using (21), with annual county level production and price statistics in the state of Montana, provided by the USDA.

Highlights

- A hydro-economic model of agricultural production written in Python is presented
- Model calibrated with stochastic version of positive mathematical programming
- Hydro-economic model can be calibrated using remote sensing observations
- A recursive Bayesian filter permits dynamic updating of model parameters
- Model predicts probabilities of land and water allocation to crops grown in a region
- Model can trace the spatial hydrologic impact of producer choices